Dalton Transactions

ROYAL SOCIETY OF CHEMISTRY

PAPER

View Article Online
View Journal | View Issue

Check for updates

Cite this: *Dalton Trans.*, 2021, **50**, 9574

Solvent-induced structural transformation from heptanuclear to decanuclear [Co–Ln] coordination clusters: trapping of unique counteranion and understanding of aggregation pathways†

Dipmalya Basak,[a] Emma Regincós Martí,[b] Mark Murrie,[b] Ivan Nemec[c,d] and Debashis Ray *[a]

Five new cobalt(II/III)–lanthanide(III)-based coordination aggregates, $[Ln^{III}_3Co^{II}_2Co^{III}_2(L1)_2(O_2CCMe_3)_8(OH)_4(OMe)_2(H_2O)_4]\cdot Ln(\eta^1\text{-}O_2CCMe_3)_2(\eta^2\text{-}O_2CCMe_3)_2(MeOH)_2\cdot 2MeOH\cdot 2H_2O$ (where Ln = Tb (**1**), Ho (**3**), and H_2L1 = *N*-(2-hydroxyethyl)-salicylaldimine), $Tb^{III}_3Co^{II}_3Co^{III}_4(L1)_4(O_2CCMe_3)_9(OH)_{10}(H_2O)$ (**4**) and $Ln^{III}_3Co^{II}_2Co^{III}_5(L1)_4(O_2CCMe_3)_{10}(OH)_{10}$ (Ln = Dy (**5**), Ho (**6**)) have been synthesized and characterized, including structural analysis *via* single-crystal X-ray diffraction. The dysprosium analogue (**2**) of **1** and **3** was previously reported by us. The heptanuclear monocationic clusters in **1** and **3** were formed by placement of seven metal ions (4 Co and 3 Ln) in a vertex shared dicubane structure from the control of two Schiff base anions and crystallized in the presence of *in situ* generated and literature unknown counter anions $Tb(\eta^1\text{-}O_2CCMe_3)_2(\eta^2\text{-}O_2CCMe_3)_2(MeOH)_2^-$ and $Ho(\eta^1\text{-}O_2CCMe_3)_2(\eta^2\text{-}O_2CCMe_3)_2(MeOH)_2^-$. Interesting solvent-induced cluster structure transformation was observed on dissolving the heptanuclear aggregates in MeCN for the formation of decanuclear clusters **4–6**. These high nuclearity clusters consist of a vertex shared heptanuclear dicubane part and a curved trinuclear chain linking the two cubic halves. The dicubane unit differs from that of the heptanuclear precursors in the presence of $Co^{II/III}$ at the shared vertex as opposed to Ln^{III} and the absence of OMe^- bridges. HRMS (+ve) analysis shed light on the pathway of formation of these heptanuclear molecules, while at the same time revealing a different aggregation process for the decanuclear clusters.

Received 18th April 2021,
Accepted 6th June 2021

DOI: 10.1039/d1dt01278a

rsc.li/dalton

Published on 22 June 2021. Downloaded by Goteborgs Universitet on 9/1/2021 4:56:06 AM.

Introduction

Surprises in dual-mode coordination chemistry and mixed metal ion structures of 3d–4f coordination aggregates have enriched synthetic chemistry in a direct way in recent years. Simple but asymmetric tridentate ONO donor ligand systems, such as sal–ea, have been known to synthetic coordination chemists for many years.[1] Schiff bases providing a central imine donor and adjacent phenol plus amino alcohol groups of varying types are known to provide both mononuclear and multinuclear complexes of 3d ions.[2] The synthesis of multimetallic 3d–4f coordination complexes can be achieved by utilizing ligands bearing two different pockets appropriate to attract two types of metal ions.[3] At the same time, ligand systems without any such clearly defined pockets have been known to hold 3d and 4f ions side-by-side within the same ligand backbone *via* utilization of bridging phenoxido, alkoxido, hydroxido, carboxylato, *etc.* groups.[4] The research in this area has attracted significant devotion due to synthetic challenges, unique structures and interesting magnetic properties. Most coordination cluster molecules are synthesized by serendipitous procedures and their formation is poorly understood.[5] Recent endeavors to understand the formation of polynuclear molecules, including metal–organic macrocycles, polyoxometalates and coordination clusters, have yielded dividends in certain cases through the utilization of mass spectrometry.[6,7] Thus, synthetic efforts can be undertaken with the anticipation

[a]*Department of Chemistry, Indian Institute of Technology, Kharagpur 721 302, India. E-mail: dray@chem.iitkgp.ac.in; Fax: (+91) 3222-82252; Tel: (+91) 3222-283324*
[b]*School of Chemistry, University of Glasgow, Glasgow, G12 8QQ, UK*
[c]*Department of Inorganic Chemistry, Faculty of Science, Palacký University, 17. listopadu 12, 77147 Olomouc, Czech Republic*
[d]*Central European Institute of Technology, CEITEC BUT, Purkyňova 656/123, 61200 Brno, Czech Republic*

†Electronic supplementary information (ESI) available: X-ray crystallographic data, Tables S1–S5, Fig. S1–S12, and Chart S1. CCDC 2061606 and 2061609–2061612 for complexes **1**, **3**, **4**, **5** and **6**. For ESI and crystallographic data in CIF or other electronic format see DOI: 10.1039/d1dt01278a

This journal is © The Royal Society of Chemistry 2021

Published on 22 June 2021. Downloaded by Goteborgs Universitet on 9/1/2021 4:56:06 AM.

of obtaining newer composition and structural types capable of providing fresh insight into the formation of such coordination aggregates.

The synthetic strategies for obtaining high nuclearity coordination clusters have attracted a lot of interest in recent times.[8] The investigation of the formation of such high nuclearity molecules is not only fascinating from a synthetic point of view, but also helps in understanding the various factors driving the aggregation process.[6c,7b,d,e] In comparison to homometallic 3d coordination cluster molecules, the literature concerning investigation into the formation of heterometallic 3d–4f clusters is extremely scarce. A very common strategy employed for the synthesis of higher nuclearity aggregates is the utilization of flexible ligand systems with multiple bridging groups. For example, the use of a Schiff base involving *o*-vanillin and *o*-aminophenol bearing adjacent ONO and OO binding sites offered a tetranuclear $Co^{II}_2Dy^{III}_2$ complex.[9] When the aminophenol backbone was replaced by amino alcohol, it resulted in clusters with increased nuclearities.[4a,10] Using even smaller and simpler ligand systems like amino alcohols and carboxylates can provide access to very high nuclearity coordination clusters purely by serendipitous means,[11] but makes it difficult to track their formation mostly due to numerous probable pathways of aggregation of initially formed species. Phenol-based Schiff bases can be useful for providing heterometallic coordination clusters having $3d_m4f_n$ cores from one-pot reactions having mixtures of 3d and 4f metal ion salts and ligand anions.[12] Tracking the formation of such coordination clusters is more feasible.[4a]

Water and solvent molecules coordinated to metal ions are activated towards hydrolysis. Ligand-controlled self-assembly leading to 3d–4f clusters can limit the degree of metal ion hydrolysis resulting in the formation of structurally well-defined hydroxide clusters. Carboxylates too are well known as time-honored ligands for the binding of lanthanide ions. Both simple carboxylates and substituted analogues like pivalates can act as hydrolysis-limiting and structure supporting co-ligands. The structure and formation of 3d–4f coordination clusters also depend on the reaction and crystallization medium. The effect of the solvent medium on the nuclearity of such aggregates has been investigated by us previously.[4a] Such solvent-induced transformation of cluster structure and nuclearity is interesting since the methodology can be utilized for the synthesis of high nuclearity clusters not accessible *via* direct reaction. The investigation of the pathway for these transformations in solution gives a wealth of information about the stability of intermediate species in various solvent mediums and the different types of aggregation processes involved. Isolation of unusual species can also be sometimes accomplished during crystallization of such aggregates.[4a,13] There have been only four examples of pure mononuclear lanthanide carboxylate anions associated with alkali metal and ammonium cations: $K_3[Er(O_2CH)_6]\cdot 2H_2O$, $K_5[Tb(O_2CH)_8]$, $(NH_4)_2[La(O_2CCH_3)_6]\cdot 0.5H_2O$ and $K_3[Yb(O_2CCH_3)_6]\cdot 4H_2O$.[14] Pure monoanionic dysprosium carboxylates associated with large heterometallic heptanuclear cationic aggregates were reported only once earlier.[4a] Recently $Co^{II/III}$-4f aggregates have attracted interest not only from a structural point of view but also due to their interesting magnetic properties.[15]

In our previous investigation using *N*-(2-hydroxyethyl)-3-methoxy-salicylaldimine, a MeCN solvent-induced transformation from heptanuclear to hexanuclear aggregates was investigated.[4a] As a continuation of that work, herein the coordination potency of the ligand *N*-(2-hydroxyethyl)-salicylaldimine (H_2L1) (Chart 1) was used, in association with *in situ* generated hydroxido and methoxido bridges and bridging pivalate ions (Chart S1†) derived from $Co_2(\mu\text{-}OH_2)(O_2CCMe_3)_4(HO_2CCMe_3)_4$, for the synthesis of mixed-valent Co-4f aggregates of two different nuclearities: heptanuclear $Ln^{III}_3Co^{II}_2Co^{III}_2$ (Ln = Tb, Ho) and decanuclear $Tb^{III}_3Co^{II}_3Co^{III}_4$ and $Ln^{III}_3Co^{II}_2Co^{III}_5$ (Ln = Dy, Ho). The Dy analogue of the heptanuclear clusters was reported earlier by us.[4a] Previously unknown counter anions $Tb(\eta^1\text{-}O_2CCMe_3)_2(\eta^2\text{-}O_2CCMe_3)_2(CH_3OH)_2^-$ and $Ho(\eta^1\text{-}O_2CCMe_3)_2(\eta^2\text{-}O_2CCMe_3)_2(CH_3OH)_2^-$, generated *in situ*, were trapped by the monocationic heptanuclear aggregates $Tb^{III}_3Co^{II}_2Co^{III+}_2$ and $Ho^{III}_3Co^{II}_2Co^{III+}_2$ during crystallization. In MeCN solution, removal of OMe^- bridges and coordinative trapping of the counter anion by ligand-bound mononuclear cobalt species led to the solvent induced structural transformation of the heptanuclear vertex-shared-dicubane cores $\{Ln^{III}_3Co^{II}_2Co^{III}_2\}$ to high nuclearity decanuclear $\{Ln^{III}_3Co^{II}_{3/2}Co^{III}_{4/5}\}$ cores. The transformed decanuclear cores can be best described as a vertex-shared-dicubane $\{Ln^{III}_2Co^{II}_{3/2}Co^{III}_{2/3}\}$ unit connected to a $\{Ln^{III}Co^{III}_2\}$ curved chain. To our knowledge, the highest known nuclearity for a Co–Ln aggregate utilizing Schiff base-type ligands is reported for a dodecanuclear $Dy^{III}_{10}Co^{II}_2$ wheel.[16] The decanuclear aggregates discussed in this work represent the highest nuclearity for mixed valent $Co^{II/III}$–Ln coordination clusters obtained using a Schiff base ligand, while at the same time possessing a unique and previously unreported topology for nuclearity ten among 3d–4f aggregates. The topology for the heptanuclear clusters has only one literature report in the Dy analogue from our lab. This is also only the second report of the utilization of H_2L1 in the synthesis of 3d–4f molecules.

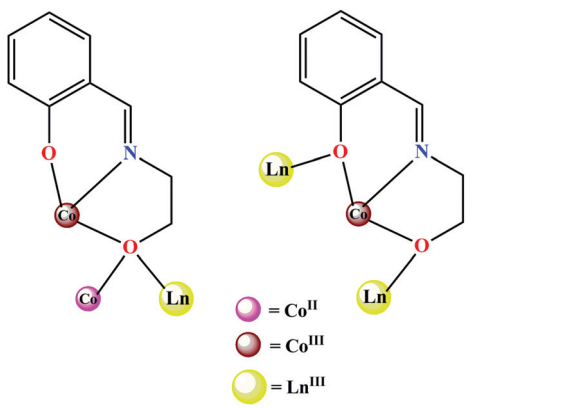

Chart 1 Structure of H_2L1 and its coordination modes observed in this work.

Published on 22 June 2021. Downloaded by Goteborgs Universitet on 9/1/2021 4:56:06 AM.

Experimental section

Reagents and starting materials

The chemicals used were obtained from the following sources: cobalt carbonate from SRL India; triethylamine from Merck, India; pivalic acid from Sigma Aldrich; $Tb(NO_3)_3{\cdot}5H_2O$, $Dy(NO_3)_3{\cdot}5H_2O$ and $Ho(NO_3)_3{\cdot}5H_2O$ from Alfa Aesar; salicylaldehyde from Spectrochem, India and 2-hydroxyethylamine from SD FineChem, India. All other chemicals and solvents used in this work were reagent grade materials and used as received without further purification.

$Co_2(\mu\text{-}OH_2)(O_2CCMe_3)_4(HO_2CCMe_3)_4$ was prepared according to a literature procedure.[17] Cobalt carbonate (4.0 g, 34 mmol) was added to an excess of pivalic acid (20.0 g, 196 mmol) in water (3 mL) at 100 °C and left to stir for 24 h, leading to its dissolution. After cooling the solution to room temperature, MeCN (50 mL) was added and stirred briefly. The solution was filtered and cooled to 5 °C, giving pink crystals within one day. After collecting the crystals, the solution was further cooled to −4 °C for 2 days to get a second crop. This too was collected by filtration, washed with cold MeCN and dried in air. Yield = 65.8%.

N-(2-Hydroxyethyl)-salicylaldimine (H_2L1) was synthesized following a previously reported literature procedure.[1c]

Synthesis of the complexes

$[Ln^{III}_3Co^{II}_2Co^{III}_2(L1)_2(O_2CCMe_3)_8(OH)_4(OMe)_2(H_2O)_4]{\cdot}Ln(\eta^1\text{-}O_2CCMe_3)_2(\eta^2\text{-}O_2CCMe_3)_2(H_2O)_2{\cdot}2MeOH{\cdot}2H_2O$ (Ln = Tb (1), Ho (3)). A general procedure was followed for the synthesis of **1** and **3**. To a MeOH (2 mL) solution of H_2L1 (0.039 g, 0.2 mmol), a MeOH (2 mL) solution of $Ln(NO_3)_3{\cdot}5H_2O$ (0.2 mmol) was added drop-wise to give a yellow solution. After stirring for 10 min, $Co_2(\mu\text{-}OH_2)(O_2CCMe_3)_4(HO_2CCMe_3)_4$ (0.095 g, 0.1 mmol) in MeOH (1 mL) was added and stirred for another 10 min, giving a red brown solution. The resulting solution was treated with Et_3N (111.2 μL, 0.4 mmol) resulting in a dark red solution and left under magnetic stirring for a period of 3 h. The precipitate was filtered off through a G4 bed and the filtrate was kept for slow evaporation of the solvent leading to good X-ray diffraction quality crystals after about a month. The synthesis of the Dy analogue (**2**) was described by us in a previous publication.[4a]

$[Tb^{III}_3Co^{II}_2Co^{III}_2]$ (1). H_2L1 (0.039 g, 0.2 mmol), $Tb(NO_3)_3{\cdot}5H_2O$ (0.090 g, 0.2 mmol), $Co_2(\mu\text{-}OH_2)(O_2CCMe_3)_4(HO_2CCMe_3)_4$ (0.095 g, 0.1 mmol), and Et_3N (111.2 μL, 0.4 mmol). Yield = 0.055 g (40% based on Tb). Anal. calcd (%) for $C_{84}H_{164}Co_4N_2O_{44}Tb_4$: C, 36.32; H, 5.95; N, 1.01. Found (%): C, 36.28; H, 5.92; N, 1.05. Selected IR peaks: (KBr, cm^{-1}, vs = very strong, br = broad, s = strong, m = medium, w = weak): 3420 (br, $\tilde{\nu}_{OH}$), 1652 (s, $\tilde{\nu}_{C=N}$), 1560 (s, asym. $\tilde{\nu}_{COO}$), 1430 (s, sym. $\tilde{\nu}_{COO}$). UV-vis: λ_{max}, nm (ε, L mol^{-1} cm^{-1}) (MeCN) = 692 (97), 594 (198), 521 (352), 405 (2920), 314 (9028), 255 (48 895).

$[Ho^{III}_3Co^{II}_2Co^{III}_2]$ (3). H_2L1 (0.039 g, 0.2 mmol), $Ho(NO_3)_3{\cdot}5H_2O$ (0.090 g, 0.2 mmol), $Co_2(\mu\text{-}OH_2)(O_2CCMe_3)_4(HO_2CCMe_3)_4$ (0.095 g, 0.1 mmol), and Et_3N (111.2 μL, 0.4 mmol). Yield = 0.056 g (41% based on Ho). Anal. calcd (%) for $C_{84}H_{164}Co_4N_2O_{44}Ho_4$: C, 36.01; H, 5.90; N, 1.00. Found (%): C, 36.00; H, 5.87; N, 1.02. Selected IR peaks: (KBr, cm^{-1}, vs = very strong, br = broad, s = strong, m = medium, w = weak): 3422 (br, $\tilde{\nu}_{OH}$), 1651 (s, $\tilde{\nu}_{C=N}$), 1558 (s, asym. $\tilde{\nu}_{COO}$), 1429 (s, sym. $\tilde{\nu}_{COO}$). UV-vis: λ_{max}, nm (ε, L mol^{-1} cm^{-1}) (MeCN) = 691 (94), 592 (193), 522 (354), 404 (2917), 312 (9022), 252 (48 885).

$Tb^{III}_3Co^{II}_3Co^{III}_4(L1)_4(O_2CCMe_3)_9(OH)_{10}(H_2O)$ (4) and $Ln^{III}_3Co^{II}_2Co^{III}_5(L1)_4(O_2CCMe_3)_{10}(OH)_{10}$ (Ln = Dy (5), Ho (6)). For the synthesis of complexes **4–6**, red block-shaped crystals of **1–3**, respectively (0.01 mmol), were treated with a 2 ml portion of MeCN to partially dissolve the respective complexes. The suspension was left to stand for half an hour and filtered. On very slow evaporation of the filtrate for a month, small red block-shaped crystals appeared which were found to be suitable for X-ray diffraction structure analysis.

$[Tb^{III}_3Co^{II}_3Co^{III}_4]$ (4). Yield: 0.0019 g (15%). Anal. calcd (%) for $C_{81}H_{129}Co_7N_4O_{37}Tb_3$: C, 36.85; H, 4.92; N, 2.12. Found (%): C, 36.80; H, 4.89; N, 2.15. Selected IR peaks: (KBr, cm^{-1}, vs = very strong, br = broad, s = strong, m = medium, w = weak): 3415 (br, $\tilde{\nu}_{OH}$), 1651 (s, $\tilde{\nu}_{C=N}$), 1553 (s, asym. $\tilde{\nu}_{COO}$), 1425 (s, sym. $\tilde{\nu}_{COO}$). UV-vis: λ_{max}, nm (ε, L mol^{-1} cm^{-1}) (MeOH) = 680 (80), 583 (200), 514 (360), 410 (2810), 310 (9130), 245 (48 780).

$[Dy^{III}_3Co^{II}_2Co^{III}_5]$ (5). Yield: 0.0020 g (15%). Anal. calcd (%) for $C_{86}H_{136}Co_7N_4O_{38}Dy_3$: C, 37.78; H, 5.01; N, 2.05. Found (%): C, 37.75; H, 4.99; N, 2.03. Selected IR peaks: (KBr, cm^{-1}, vs = very strong, br = broad, s = strong, m = medium, w = weak): 3408 (br, $\tilde{\nu}_{OH}$), 1650 (s, $\tilde{\nu}_{C=N}$), 1554 (s, asym. $\tilde{\nu}_{COO}$), 1426 (s, sym. $\tilde{\nu}_{COO}$). UV-vis: λ_{max}, nm (ε, L mol^{-1} cm^{-1}) (MeOH) = 682 (83), 580 (203), 514 (366), 414 (2817), 312 (9134), 247 (48 786).

$[Ho^{III}_3Co^{II}_2Co^{III}_5]$ (6). Yield: 0.0020 g (15%). Anal. calcd (%) for $C_{86}H_{136}Co_7Ho_3N_4O_{38}$: C, 37.68; H, 5.00; N, 2.04. Found (%): C, 37.70; H, 4.97; N, 2.01. Selected IR peaks: (KBr, cm^{-1}, vs = very strong, br = broad, s = strong, m = medium, w = weak): 3410 (br, $\tilde{\nu}_{OH}$), 1650 (s, $\tilde{\nu}_{C=N}$), 1553 (s, asym. $\tilde{\nu}_{COO}$), 1423 (s, sym. $\tilde{\nu}_{COO}$). UV-vis: λ_{max}, nm (ε, L mol^{-1} cm^{-1}) (MeOH) = 683 (78), 584 (196), 516 (364), 412 (2808), 309 (9128), 244 (48 789).

Physical measurements

A PerkinElmer model 240C elemental analyzer was used to perform elemental analyses (C, H and N). FTIR spectra were measured on a PerkinElmer RX1 spectrometer while a Shimadzu UV 3100 UV/Vis/NIR spectrophotometer was used to record the solution electronic absorption spectra. A Bruker Daltonics micrOTOF mass spectrometer was employed to collect the electrospray ionization (ESI) high resolution mass spectra to understand the formation and transformation of the coordination clusters.

SQUID measurements

All magnetic measurements were carried out on powdered crystalline samples restrained in eicosane using a Quantum Design MPMS 3 SQUID magnetometer. Data were corrected for the diamagnetic contribution of the sample holder and eicosane by measurements, and for the diamagnetism of each compound.

 This journal is © The Royal Society of Chemistry 2021

Published on 22 June 2021. Downloaded by Goteborgs Universitet on 9/1/2021 4:56:06 AM.

Crystal data collection and refinement

Single crystal X-ray diffraction data for **1**, **3**, and **4–6** were collected on a Bruker SMART APEX-III CCD X-ray diffractometer furnished with graphite-monochromated Mo Kα (λ = 0.71073 Å) radiation by the ω scan (width of 0.3° frame^{-1}) method at 293–300 K with a scan rate of 4 s per frame. SAINT and XPREP software[18] were used for data processing and space group determination. The structure was solved using the direct method of SHELXS-2014[19] and then refined with full-matrix least squares using the SHELXL-(2014/7)[20] program package included in WINGX system Version 2014[21] and Olex2 Version 1.2.[22] Data were corrected for Lorentz and polarization effects; an empirical absorption correction was applied using SADABS.[23] The locations of the heaviest atoms (Ln and Co) were determined easily. The O, N, and C atoms were subsequently determined from the difference Fourier maps. These atoms are refined anisotropically. The H atoms were incorporated at calculated positions and refined with fixed geometry and riding thermal parameters with respect to their carrier atoms. Some of the crystals showed somewhat weak diffraction and diffuse scattering. The electron density peak of 4.780 e at about 1.880 Å from Co3 and 1.515 Å from O15 in **6** could not be modeled as any sensible species and was considered as an absorption artifact. Crystallographic diagrams were presented using DIAMOND software.[24] A summary of the crystal data and relevant refinement parameters is summarized in Table 1. Crystallographic data (including structure factors) have been deposited with the Cambridge Crystallographic Data Centre as supplementary publications CCDC – 2061606 and 2061609–2061612.†

Results and discussion

Synthetic methodology

2-{(2-Hydroxyethyl)imino}methylphenol (H_2L1) was obtained through the condensation of salicylaldehyde and 2-hydroxyethylamine in a 1 : 1 molar ratio under refluxing conditions. The coordinative reactivity of H_2L1 in MeOH toward $Ln(NO_3)_3{\cdot}5H_2O$ and $Co_2(\mu\text{-}OH_2)(O_2CCMe_3)_4(HO_2CCMe_3)_4$ in the presence of NEt_3 and MeCN-induced structural transformation have been examined to obtain products of two different types having aggregate structures as summarized in Scheme 1. The reaction of H_2L1 with $Ln(NO_3)_3{\cdot}5H_2O$ (Ln = Tb, Ho) and $Co_2(\mu\text{-}OH_2)(O_2CCMe_3)_4(HO_2CCMe_3)_4$ in the presence of NEt_3 in 1 : 0.5 : 1 : 4 molar ratio in MeOH resulted in red-brown solutions, from which red block-shaped single crystals of **1** and **3** were obtained in 40% and 41% yields, respectively (eqn (1)). Single-crystal X-ray structure analysis revealed the formation of cationic heptanuclear $\{Ln^{III}_3Co^{II}_2Co^{III}_2\}$ cores in **1** (Tb) and **3** (Ho) from the coordination control of two ligand anions. Elemental analysis and physical characterizations were in good agreement with the molecular formulae $C_{84}H_{164}Co_4N_2O_{44}Tb_4$ and $C_{84}H_{164}Co_4N_2O_{44}Ho_4$ for **1** and **3**, respectively, and the cationic nature of the complexes. During crystallization, the previously unreported anionic species $Tb(\eta^1\text{-}O_2CCMe_3)_2(\eta^2\text{-}O_2CCMe_3)_2(CH_3OH)_2^-$ and $Ho(\eta^1\text{-}O_2CCMe_3)_2(\eta^2\text{-}O_2CCMe_3)_2(CH_3OH)_2^-$ were generated *in situ* from the reaction medium and were crucial for the growth of the crystals of **1** and **3** serving as counter anions to the cationic $\{Ln^{III}_3Co^{II}_2Co^{III}_2\}$ cores. Coordination of imine-centered $L1^{2-}$ to $Co_2(\mu\text{-}OH_2)$

Table 1 Crystal data and structure refinement details for **1**, **3**, **4**, **5** and **6**

Compound	**1**	**3**	**4**	**5**	**6**
Formula	$C_{84}H_{164}Co_4N_2O_{44}Tb_4$	$C_{84}H_{164}Co_4N_2O_{44}Ho_4$	$C_{81}H_{129}Co_7N_4O_{37}Tb_3$	$C_{86}H_{136}Co_7N_4O_{38}Dy_3$	$C_{86}H_{136}Co_7N_4O_{38}Ho_3$
F.W. (g mol^{-1})	2777.58	2801.58	2640.14	2734.01	2741.30
Crystal system	Monoclinic	Monoclinic	Monoclinic	Monoclinic	Monoclinic
Space group	*P*2/*n*	*P*2/*n*	$P2_1/n$	*C*2/*c*	*C*2/*c*
Crystal color	Red	Red	Red	Red	Red
Crystal size/mm^3	0.23 × 0.20 × 0.19	0.25 × 0.23 × 0.22	0.15 × 0.14 × 0.12	0.16 × 0.15 × 0.14	0.16 × 0.15 × 0.13
a/Å	19.1693(9)	19.075(3)	17.9546(11)	18.1864(11)	18.1767(11)
b/Å	12.4008(7)	12.3733(18)	38.827(2)	38.561(2)	38.392(2)
c/Å	27.0683(13)	27.043(4)	18.5890(12)	18.5641(11)	18.6387(10)
α	90°	90°	90°	90°	90°
β	107.573(3)°	107.465(5)°	113.214(3)°	108.441(3)°	108.166(2)°
γ	90°	90°	90°	90°	90°
V/Å^3	6134.2(5)	6088.4(16)	11 909.7(12)	12 350.3(13)	12 358.7(13)
Z	2	2	4	4	4
D_c/g cm^{-3}	1.504	1.526	1.472	1.470	1.473
μ/mm^{-1}	2.875	3.172	2.773	2.774	2.879
F(000)	2804	2812	5292	5484	5496
T/K	298(2)	296(2)	293(2)	300(2)	296(2)
Total reflns	46 499	94 615	90 447	47 139	100 001
R(int)	0.0459	0.0743	0.1431	0.0844	0.0513
Unique reflns	10 874	10 806	20 922	10 999	12 676
Observed reflns	8043	8719	10 076	5523	7747
Parameters	678	675	1360	647	654
R_1; wR_2 ($I > 2\sigma(I)$)	0.0502, 0.1510	0.0509, 0.1438	0.0781, 0.2491	0.0892, 0.3104	0.0912, 0.2737
GOF (F^2)	1.086	1.052	1.001	1.038	1.090
Largest diff peak and hole (e Å^{-3})	1.779, −2.162	1.601, −1.826	1.141, −1.698	2.088, −1.940	4.780, −2.839
CCDC no.	2061606	2061609	2061610	2061611	2061612

Published on 22 June 2021. Downloaded by Goteborgs Universitet on 9/1/2021 4:56:06 AM.

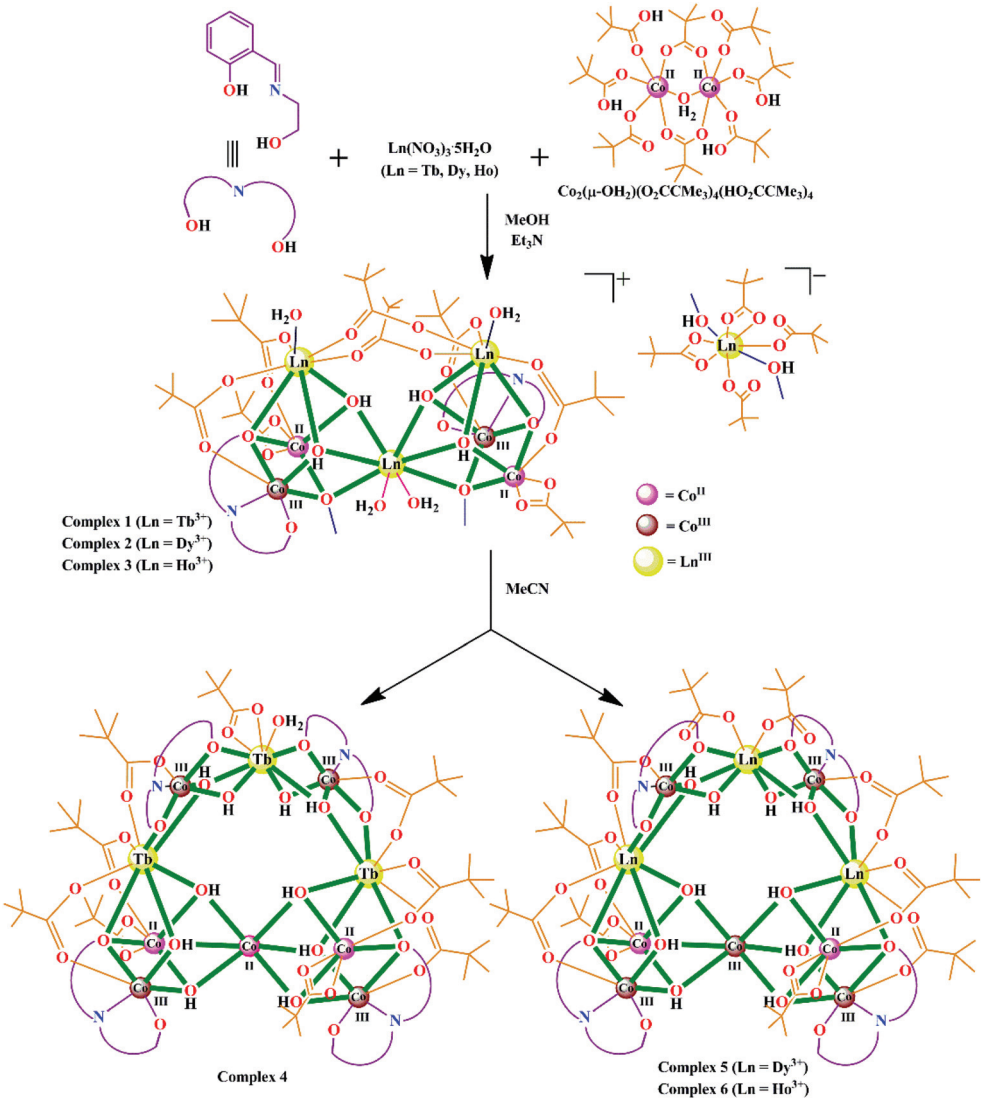

Scheme 1 Synthesis of **1–3** and their transformation to **4–6**.

$(O_2CCMe_3)_4(HO_2CCMe_3)_4$ gave a methoxido bridged $\{Co_2\}$ species, which further traps a Ln^{III} ion forming a $\{Co_2Ln\}$ species. Two such $\{Co_2Ln\}$ fragments having facial O_3 bridging sites made from two HO^- and one OMe^- finally entrap one Ln^{III} center to provide the cationic cores of **1** and **3**.

$$\begin{aligned} &4H_2L1 + 4Co_2(\mu\text{-}OH_2)(O_2CCMe_3)_4(HO_2CCMe_3)_4 \\ &+ 8Ln(NO_3)_3 \cdot 5H_2O + 24NEt_3 + 12MeOH \\ &+ O_2 \xrightarrow{CH_3OH} 2[Ln^{III}_3Co^{II}_2Co^{III}_2(L1)_2(O_2CCMe_3)_8 \\ &(OH)_4(OMe)_2(H_2O)_4] \cdot Ln(\eta^1\text{-}O_2CCMe_3)_2 \\ &(\eta^2\text{-}O_2CCMe_3)_2(MeOH)_2 \cdot 2MeOH \cdot 2H_2O \\ &+ 24\{(NHEt_3)(NO_3)\} + 8HO_2CCMe_3 \\ &+ 26H_2O(Ln = Tb^{3+}, Ho^{3+}). \end{aligned} \quad (1)$$

Separated crystals of **1** and **3** along with the previously reported **2** on treatment with MeCN gave red suspensions, which were allowed to stand for half an hour and then filtered. Red block-shaped crystals of **4–6** were formed after a month in 15% yields when the filtrates were allowed to evaporate very slowly (eqn (2) and (3)). Single-crystal X-ray structure analysis revealed the formation of decanuclear $\{Tb^{III}_3Co^{II}_3Co^{III}_4\}$, $\{Dy^{III}_3Co^{II}_2Co^{III}_5\}$ and $\{Ho^{III}_3Co^{II}_2Co^{III}_5\}$ core-bearing clusters **4**, **5** and **6**, respectively. Dissolution of **1**, **2** and **3** in MeCN led to the removal of the OMe^- bridges and central lanthanide ion for the disintegration of the heptanuclear $\{Ln^{III}_3Co^{III}_2Co^{II}_2\}$ (Ln = Tb, Dy, Ho) cores. Unique restructuring to higher order decanuclear aggregates was initiated by: (1) the entrapment of the bare $Co^{II/III}$ center at the vertex shared position of the Ln^{III} ion by two trinuclear $\{Co_2Ln\}$ species (formed after collapse of the heptanuclear core) forming the dicubane part and (2) trapping of the unique counter anion $Ln(\eta^1\text{-}O_2CCMe_3)_2(\eta^2\text{-}O_2CCMe_3)_2(MeOH)_2^-$ by two mononuclear $\{Co^{III}L1\}$ species (generated after further dissociation of some $\{Co_2Ln\}$ frag-

 This journal is © The Royal Society of Chemistry 2021

Published on 22 June 2021. Downloaded by Goteborgs Universitet on 9/1/2021 4:56:06 AM.

ments) forming the curved chain part. Coordination driven aggregation of these two units led to the formation of **4–6** as solid crystals. The trinuclear $\{Co_2Ln\}$ species formed in MeCN does not possess the bridging methoxido group compared to that in MeOH during synthesis of **1–3**, further reflected by its absence in the dicubane portion of **4–6**. The importance of the bridging OMe^- in trapping the Ln^{III} ion at the shared vertex in **1–3** is exemplified by this transformation. Elemental analysis data also gave $C_{81}H_{129}Co_7N_4O_{37}Tb_3$, $C_{86}H_{136}Co_7N_4O_{38}Dy_3$ and $C_{86}H_{136}Co_7N_4O_{38}Ho_3$ as the molecular formula for **4**, **5** and **6**, respectively.

$$\begin{aligned} &2Tb_3^{III}Co_2^{II}Co_2^{III}(L1)_2(O_2CCMe_3)_8(OH)_4(OMe)_2\\ &(H_2O)_4\cdot Tb(\eta^1\text{-}O_2CCMe_3)_2(\eta^2\text{-}O_2CCMe_3)_2\\ &(MeOH)_2\cdot 2MeOH\cdot 2H_2O \xrightarrow{MeCN} [Tb_3^{III}Co_3^{II}\\ &Co_4^{III}(L1)_4(O_2CCMe_3)_9(OH)_{10}(H_2O)] + 5Tb^{III}\\ &+ Co^{II} + 15Me_3CCO_2^- + 4OMe^- + 2H^+\\ &+ 8MeOH + 9H_2O \end{aligned} \quad (2)$$

$$\begin{aligned} &8Ln_3^{III}Co_2^{II}Co_2^{III}(L1)_2(O_2CCMe_3)_8(OH)_4(OMe)_2\\ &(H_2O)_4\cdot Ln(\eta^1\text{-}O_2CCMe_3)_2(\eta^2\text{-}O_2CCMe_3)_2\\ &(MeOH)_2\cdot 2MeOH\cdot 2H_2O + O_2 \xrightarrow{MeCN}\\ &4[Ln_3^{III}Co_2^{II}Co_5^{III}(L1)_4(O_2CCMe_3)_{10}(OH)_{10}] + 20Ln^{III}\\ &+ 4Co^{II} + 56Me_3CCO_2^- + 16OMe^- + 4H^+\\ &+ 32MeOH + 42H_2O (Ln = Dy^{3+}, Ho^{3+}). \end{aligned} \quad (3)$$

Description of the crystal structures

$[Ln_3^{III}Co_2^{II}Co_2^{III}(L1)_2(O_2CCMe_3)_8(OH)_4(OMe)_2(H_2O)_4]\cdot Ln(\eta^1\text{-}O_2CCMe_3)_2(\eta^2\text{-}O_2CCMe_3)_2(MeOH)_2\cdot 2MeOH\cdot 2H_2O$ (Ln = Tb (1), Ho (3)). Both the aggregates **1** and **3** crystallize in the monoclinic $P2/n$ space group with $Z = 2$. Chosen bond distances and bond angles are listed in Table S1.† The perspective view of the cationic part of the structures for **1** and **3** is shown in Fig. 1 and consists of a heptanuclear $\{Ln_3Co_4\}$ core $Ln_3^{III}Co_2^{II}Co_2^{III}(L1)_2(O_2CCMe_3)_8(OH)_4(OMe)_2(H_2O)_4^+$. Within the reaction medium, scrambling of pivalate ions took place between $Co_2(\mu\text{-}OH_2)(O_2CCMe_3)_4(HO_2CCMe_3)_4$ and $Ln(NO_3)_3\cdot 5H_2O$ to yield the hitherto unknown anionic species $Tb(\eta^1\text{-}O_2CCMe_3)_2(\eta^2\text{-}O_2CCMe_3)_2(MeOH)_2^-$ and $Ho(\eta^1\text{-}O_2CCMe_3)_2(\eta^2\text{-}O_2CCMe_3)_2(MeOH)_2^-$ which are trapped in the crystal lattice for charge compensation in **1** and **3**, respectively (Fig. 3). Two molecules of water and methanol each are present in both the lattices. As the aggregates are isostructural, the discussion of the structure is given in short mainly with respect to **1** as a representative case.

The analysis of the X-ray structure revealed that in each half of the vertex-shared dicubane $\{Ln_3^{III}Co_2^{II}Co_2^{III}\}$ clusters, a $L1^{2-}$ anion coordinates a Co^{III} center in its ONO site, while at the same time bridging another Co^{II} and Ln^{III} ion through its μ_3 alcohol arm. One OMe^- and two OH^- μ_3-bridges from each half were responsible for attracting the Ln^{III} in the vertex shared position. Cover up $\mu_{1,3}$-bridging by six pivalate ions derived from $Co_2(\mu\text{-}OH_2)(O_2CCMe_3)_4(HO_2CCMe_3)_4$ was crucial for stabilizing the bent dicubane structure. The OMe^- bridges are important for the incorporation of the vertex shared Ln^{III} ion and directing the ultimate structure of the cluster and will be discussed further in subsequent sections. Fig. 2 represents the core structure of **1** highlighting the bond distances and intermetallic distances. A more detailed description is given in the ESI.†

Crystallization of the cationic parts of the Co–Ln aggregates was achieved through *in situ* generation of the unique charge-compensating anions $Tb^{III}(\eta^1\text{-}O_2CCMe_3)_2(\eta^2\text{-}O_2CCMe_3)_2(MeOH)_2^-$ and $Ho^{III}(\eta^1\text{-}O_2CCMe_3)_2(\eta^2\text{-}O_2CCMe_3)_2(MeOH)_2^-$ in **1** and **3**. In solution, reaction of lanthanide(III) ions with Co_2–pivalate precursor provided these literature unknown anions suitable for crystal packing. The rareness of mononuclear carboxylate anions of lanthanide elements is exemplified by there being only four known examples in association with alkali metal and ammonium cations[14] and a previous report of a similar dysprosium(III)–pivalate-based anion.[4a] In **1**, the anion consists of a Tb^{III} ion (Tb3) in O_8 coordination geometry being

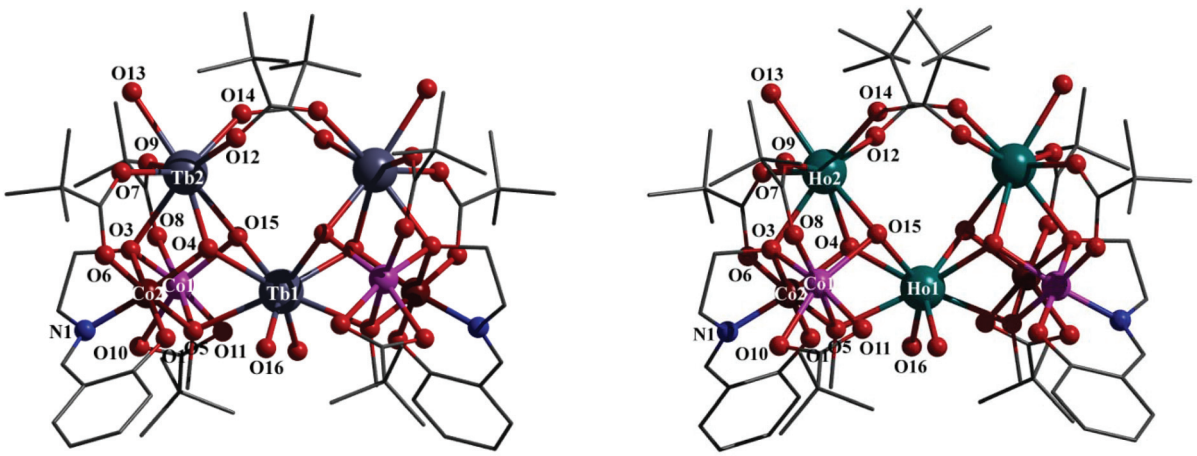

Fig. 1 Molecular structures of the cationic parts of **1** (left) and **3** (right). Hydrogen atoms and solvent molecules are omitted for clarity. Color code: grey, carbon; red, oxygen; blue, nitrogen; blue grey, terbium; teal, holmium, pink, cobalt(II); brown, cobalt(III).

Published on 22 June 2021. Downloaded by Goteborgs Universitet on 9/1/2021 4:56:06 AM.

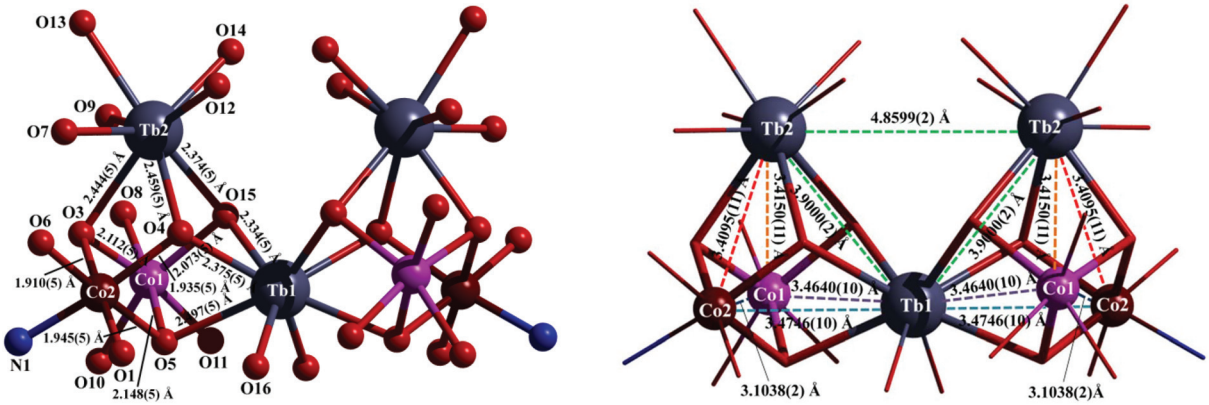

Fig. 2 Core structure of **1** with bond distances (left) and the intermetallic separation within the core (right). Carbon and hydrogen atoms are omitted for clarity. Color code: red, oxygen; blue, nitrogen; blue grey, terbium; pink, cobalt(II); brown, cobalt(III).

coordinated by two η^1-$Me_3CCO_2^-$ ions, two η^2-$Me_3CCO_2^-$ ions and two MeOH molecules. The Tb3–O distances of 2.308(7) Å for η^1-$Me_3CCO_2^-$ (O19) are shorter than those of η^2-$Me_3CCO_2^-$ (O18, O17) at 2.369(7) and 2.387(7) Å, while the MeOH records the largest Tb3–O21 distance of 2.394(6) Å. From the CShM values (CShM = 2.272 for TDD, 3.044 for BTPR, 3.759 for SAPR) the geometry around Tb3 is best defined as a distorted triangular dodecahedron (Table S4† and Fig. 3). Similar observations were made for Ho3 in **3**.

Inter and intra-molecular hydrogen bonding interactions as structure stabilizing secondary connections play an important role providing stability to the dicubane cores and trapping of the unique lanthanide(III)–pivalate-based counter anions (Table S5† and Fig. 4). A detailed description of the hydrogen bonded 1D chain structure is presented in the ESI.†

$Tb^{III}_3Co^{II}_3Co^{III}_4(L1)_4(O_2CCMe_3)_9(OH)_{10}(H_2O)$ (4) and $Ln^{III}_3Co^{II}_2Co^{III}_5(L1)_4(O_2CCMe_3)_{10}(OH)_{10}$ (Ln = Dy (5), Ho (6)). The transformed cluster **4** crystallizes in the monoclinic $P2_1/n$ space group with $Z = 4$, while **5** and **6** crystallize in the monoclinic $C2/c$ space group with $Z = 4$. Selected metric parameters are presented in Table S1.† The molecular structures of **4–6** consist of only the charge-neutral $Tb^{III}_3Co^{II}_3Co^{III}_4(L1)_4(O_2CCMe_3)_9(OH)_{10}(H_2O)$ and $Ln^{III}_3Co^{II}_2Co^{III}_5(L1)_4(O_2CCMe_3)_{10}(OH)_{10}$ (Ln = Dy, Ho) units with variation in the number of coordinating $Me_3CCO_2^-$ anions and Co^{II} and Co^{III} centers. The molecular structure of **4–6** is presented in Fig. 5. The following structural description involves **4** and mainly **6**, which is isostructural with **5**.

The structures of **4–6** consist of a vertex-shared dicubane moiety $\{Ln^{III}_2Co^{II}_3Co^{III}_2\}$ (**4**)/$\{Ln^{III}_2Co^{II}_2Co^{III}_3\}$ (**5**, **6**) with a curved chain $\{Ln^{III}Co^{III}_2\}$ connecting both Ln^{III} ends of the dicubane unit (Fig. 6). The overall getup of the dicubane part is similar to that observed in the case of **1–3** with the substitution of the μ_3-OMe^- bridges by OH^- ions and the Ln^{III} ion at the vertex-

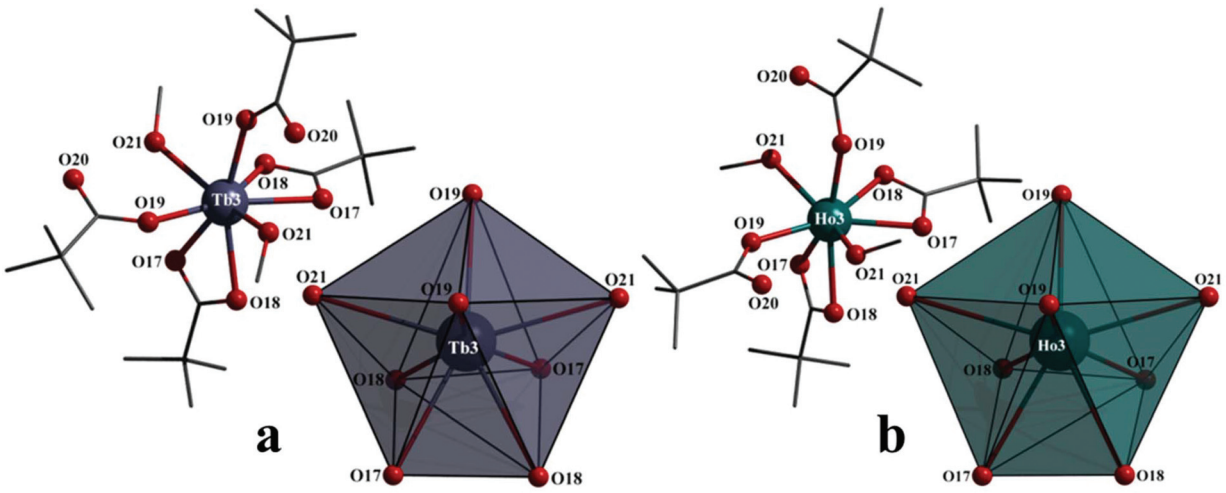

Fig. 3 Structure of the Tb^{III} and Ho^{III}–pivalate-based counteranion present in **1** (a, left) and **3** (b, left) and the distorted trigonal dodecahedral coordination geometry around Tb3 (a, right) and Ho3 (b, right). Hydrogen atoms and solvent molecules are omitted for clarity. Color code: grey, carbon; red, oxygen; blue grey, terbium; teal, holmium.

 This journal is © The Royal Society of Chemistry 2021

Published on 22 June 2021. Downloaded by Goteborgs Universitet on 9/1/2021 4:56:06 AM.

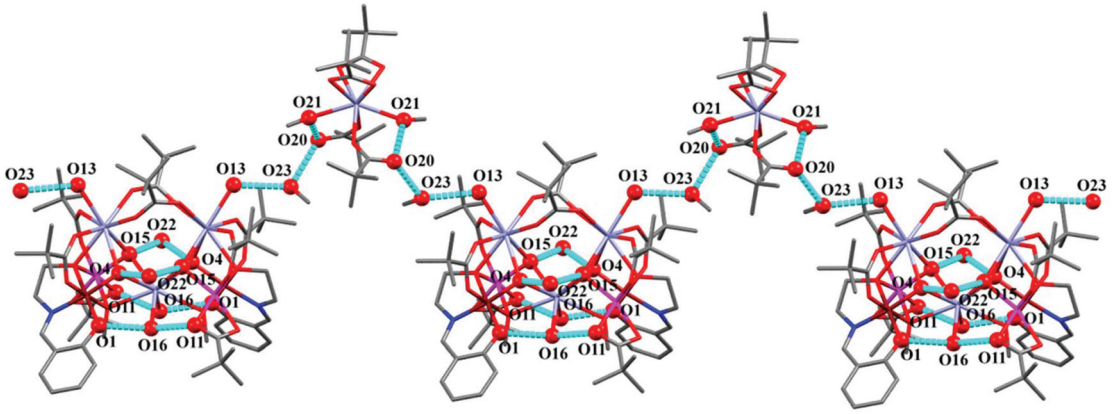

Fig. 4 1D chain structure in **1** formed by the trapping of $Tb^{III}(\eta^1\text{-}O_2CCMe_3)_2(\eta^2\text{-}O_2CCMe_3)_2(MeOH)_2^-$ and solvent molecules through hydrogen bonded interactions.

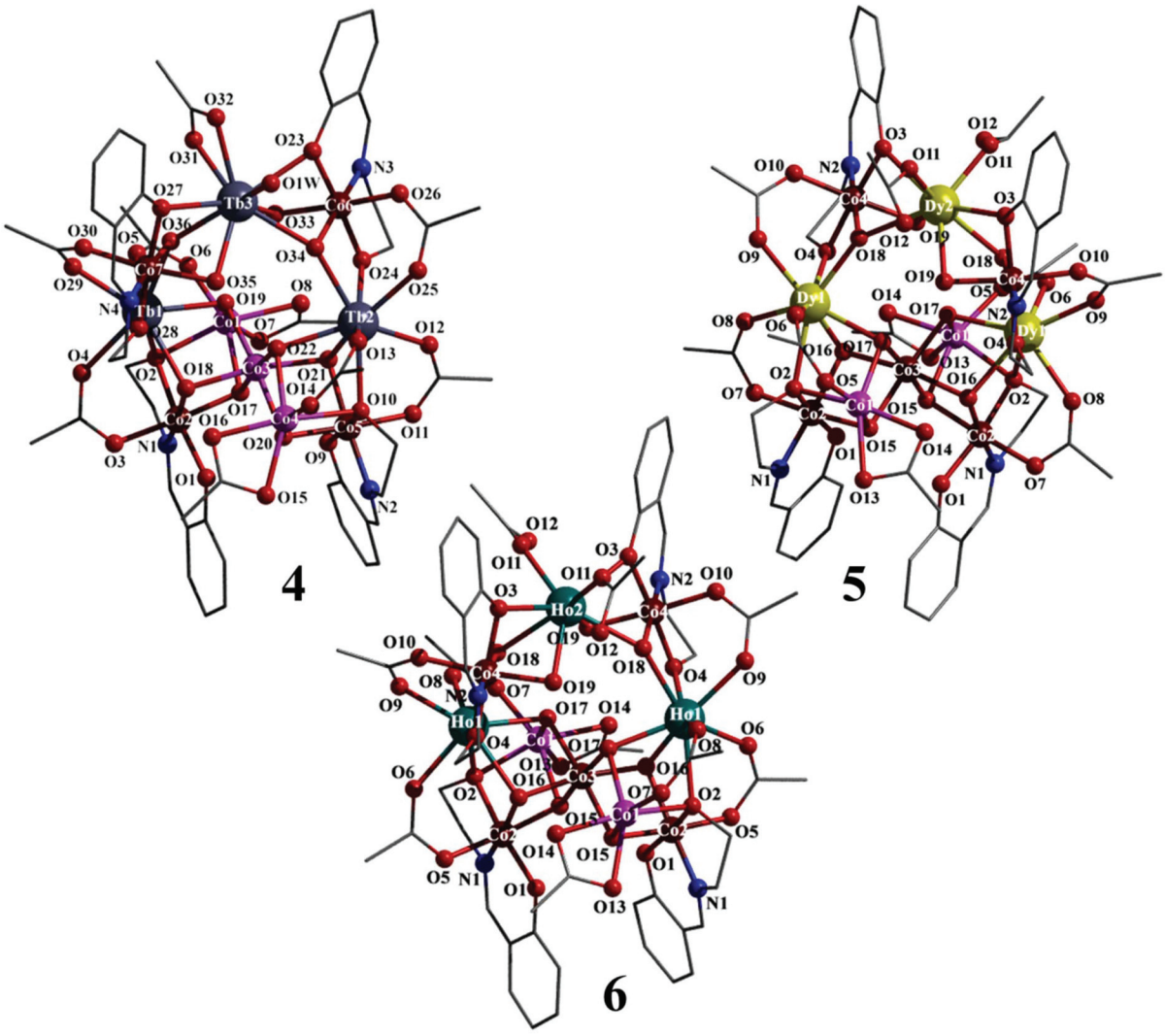

Fig. 5 Molecular structures of **4**–**6**. Hydrogen atoms and methyl groups on pivalate omitted for clarity. Color code: grey, carbon; red, oxygen; blue, nitrogen; blue grey, terbium; yellow, dysprosium; teal, holmium; pink, cobalt(II); brown, cobalt(III).

Published on 22 June 2021. Downloaded by Goteborgs Universitet on 9/1/2021 4:56:06 AM.

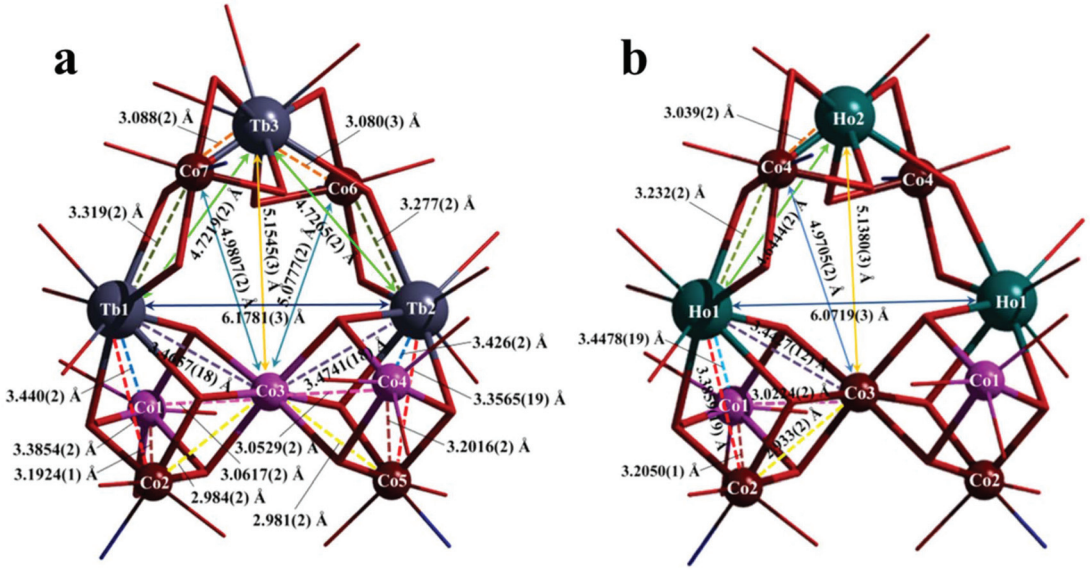

Fig. 6 Core structures of **4** (a) and **6** (b) with intermetallic separation within the cores. Carbon atoms omitted for clarity. Color code: grey, carbon; red, oxygen; blue, nitrogen; blue grey, terbium; teal, holmium; pink, cobalt(II); brown, cobalt(III).

shared position by Co^{II} (Co3) in **4** and Co^{III} (Co3) in **5–6**. In the presence of MeCN the structural supports of μ_3-OMe^- in **1–3** were lost leading to the collapse of the clusters with removal of the shared Ln^{III}. From the molecular fragments formed by this disintegration of **1–3**, a different route of aggregation evolved leading to the growth and crystallization of **4–6** as discussed in the following section. Each cubic half of the heptanuclear dicubane $\{Ln^{III}_2Co^{II}_{3/2}Co^{III}_{2/3}\}$ part consists of a $L1^{2-}$ anion coordinated to Co^{III} and extending the alcohol arm to further bridge a second Co^{II} and a Ln^{III} ion in the μ_3-bridging mode. Three μ_3-OH^- bridges in each half were further utilized to attract another $Co^{II/III}$ ion at the vertex shared position. Four ancillary $\mu_{1,3}$-pivalate bridges further support the outer Ln^{III}–Co^{III} and Ln^{III}–Co^{II} faces, while two others show a η^2 chelation towards the Co^{II} centers. The $\{Ln^{III}Co^{III}_2\}$ chain consists of two $L1^{2-}$ anions coordinated to a Co^{III} ion each in their tridentate ONO binding site. Two $\{Co^{III}L1\}$ units trap the unique lanthanide–pivalate-based counter anion present in **1–3** through μ_2-bridging phenoxido groups along with four OH^- bridges. The μ_2-bridging alcohol arm of $L1^-$ and two μ_2-OH^- and two μ_3-OH^- bridges were utilized to connect the $\{LnCo_2\}$ chain to the $\{Ln_2Co_5\}$ dicubane unit at the Ln^{III} positions. The connection is further stabilized *via* two $\mu_{1,3}$-$Me_3CCO_2^-$ bridges between Ln^{III} and Co^{III} ions. Interestingly the chelating coordination of one $Me_3CCO_2^-$ anion and a water molecule put the chain Tb^{III} center in an $\{O_9\}$ coordination environment in **4**, whereas in the cases of **5** and **6**, monodentate coordination of two $Me_3CCO_2^-$ anions results in $\{O_8\}$ coordination environments around the Dy^{III} and Ho^{III} ions.

Within the $\{Co_3Tb\}$ cubes in **4**, the shortest intermetallic separation is observed at 2.984(2) Å (Co_2···Co3) and 2.981(2) Å (Co3···Co5) (Fig. 6a), while the longest separations amount to 3.4657(18) (Tb1···Co3) and 3.4741(18) Å (Tb2···Co3). For **6**, the smallest separation is at 2.933(2) Å (Co_2···Co3), but the longest separation of 3.4478(19) Å is recorded between Ho1 and Co1 and not the shared Co3 (Fig. 6b). Of the three TbO_2Co faces on each cubic half in **4**, the separation between the doubly bridged Tb and Co centers is longer (Tb1···Co3, 3.4661(2) Å; Tb2···Co3, 3.4729(1) Å) than the triply bridged ones (Tb1···Co1, 3.4657(18) Å; Tb1···Co_2, 3.3845(19) Å; Tb2···Co4, 3.426(2) Å; Tb2···Co5, 3.3565(19) Å). In **6**, the doubly bridged Ho1···Co3 distance at 3.4427(12) Å is intermediate between the triply bridged Ho1···Co1 (3.4478(19) Å) and Ho1···Co_2 (3.3859 (19) Å) separations. The Tb1···Tb2 separation in **4** and Ho1···Ho1 separation in **6** at 6.1781(3) Å and 6.0719(3) Å are the longest within the dicubane unit and much longer than the analogous distances in **1** and **3** pointing to less bending of the dicubane in the transformed clusters mostly due to the trapping of a O_6 3d ion in place of the O_8 4f ion at the shared vertex. Within the $\{Co_2Ln\}$ chain, the separation of Co^{III} from the Ln^{III} (Tb3···Co6, 3.080(3) Å; Tb3···Co7, 3.088(2) Å in **4** and Ho2···Co4, 3.039(2) Å in **6**) is smaller than that from the cube Ln^{III} (Tb2···Co6, 3.277(2) Å; Tb1···Co7, 3.319(2) Å in **4** and Ho1···Co4, 3.232(2) Å in **6**). The distances between the Ln^{III} ions in the chain and the cubic halves (Tb3···Tb1, 4.7219(2) Å; Tb3···Tb2, 4.7265(2) Å in **4** and Ho2···Ho1, 4.6444(2) Å in **6**) were much shorter than those within the dicubane moiety (see above).

Fig. S4† presents the various bond distances within the cores of **4** and **6**. In **6**, the Co–O_{hyd}–Ho (hy = hydroxido) angles within the dicubane moiety are spread over a narrow range from 101.6(3)° (Co_2–O16–Ho1) to 104.7(4)° (Co3–O17–Ho1) with the Co^{II}–O_{alk}–Ho (alk = alkoxido) angle of 95.3(3)° (Co1–O2–Ho1) being smaller than the Co^{III}–O_{alk}–Ho angle at 101.1 (3)° (Co_2–O2–Ho1). The Co–O–Co angles vary over a wide range from 94.9(4)° to 105.6(4)°. Within the chain in **6**, the Co4–

 This journal is © The Royal Society of Chemistry 2021

Published on 22 June 2021. Downloaded by Goteborgs Universitet on 9/1/2021 4:56:06 AM.

O18–Ho1 angle (96.2(4)°) involving the μ_3-OH^- bridge is larger than the Co4–O18–Ho2 angle (87.5(3)°) while the Ho1–O18–Ho2 angle at 147.5(4)° is very wide. The μ_2-OH^- bridge recorded a shorter Co4–O19–Ho2 angle of 91.2(4)° compared to the 102.2(4)° for Co4–O4–Ho1 involving μ_2-alkoxido. For the μ_2-phenoxido bridge the angle stands at 88.8(4)° (Co4–O3–Ho2). Similar observations regarding bond angles were made in the case of **4**. bond valence sum (BVS)[25,26] analysis for localized bonds around the metal ion centers validated a formal valence state of +II for Co1, Co3 and Co4 in **4** and for Co1 and Co4 in **5** and **6** while a +III valence state could be assigned to Co_2, Co5, Co6, Co7, Tb1, Tb2 and Tb3 in **4** and Co_2, Co3, Co4, Ln1 and Ln2 in **5** and **6** (Table S2†).

To investigate the O_8/O_9 coordination geometry around Ln^{III} and the O_6/O_5N geometry around $Co^{II/III}$ ions in **4–6**, continuous shape measures (CShM) calculations were performed (Tables S3 and S4†). In the case of **4**, the geometry around both the eight coordinated Tb1 and Tb2 is close to a square antiprism (SAPR) (CShM (Tb1) = 0.666 for SAPR, 1.834 for BTPR, 2.241 for TDD; CShM (Tb2) = 0.416 for SAPR, 1.818 for BTPR, 2.289 for TDD) while that around the nine coordinated Tb3 (curved chain) is best described as a distorted muffin (CShM = 0.874 for MFF, 1.796 for CSAPR, 2.536 for TCTPR) as is evident from the lower CShM values (Fig. 7, top and Table S4†). In **6**, the octa coordinated Ho1 exhibits a distorted SAPR geometry (CShM = 0.518 for SAPR, 1.663 for BTPR, 2.005 for TDD) while the other octa coordinated Ho2 in the chain adopts a distorted TDD geometry (CShM = 1.161 for TDD, 2.000 for BTPR, 2.346 for SAPR) (Fig. 7, bottom and Table S4†). Similar observations were made in the case of Dy1 and Dy2 in **5**. The difference in coordination number and geometry of the Ln^{III} ion in the curved chain of **4** compared to **5** and **6** leads to subtle distortion of the octahedral geometry around the Co3 center (percolating through the whole structure) at the vertex-shared position in **4** stabilizing it in the +II valence state as opposed to the +III state in **5** and **6**. The cobalt ion in its +II valence state is known to accommodate much higher distortion of the octahedral geometry compared to the +III valence state.[3] The CShM values of Co3 in the three structures confirms this distortion (1.233 (**4**) > 0.992 (**5**) ≈ 0.946 (**6**)) (*vide infra*). The preference of lower coordination number of Dy^{III} and Ho^{III} in comparison to Tb^{III} in the chain arises as a result of lanthanide contraction.

A uniform Octahedral coordination environment around all Co centers in **4–6** is confirmed from the CShM values. In **4**, the higher CShM values for bivalent Co1 (4.371) and Co4 (3.854) point to a higher distortion of the octahedral geometry compared to trivalent Co_2 (0.272), Co5 (0.286), Co6 (0.305) and Co7 (0.281) (Fig. S5 and Table S3†). A similar trend is observed in **5–6** with bivalent Co1 (CShM = 4.123 (**5**), 4.154 (**6**)) showing comparatively higher distortion than trivalent Co2 (CShM = 0.329 (**5**), 0.338 (**6**)) and Co4 (CShM = 0.205 (**5**), 0.216 (**6**)) (Fig. S6†). The Co3 at the vertex shared position showed less distortion (CShM = 1.233) compared to other divalent Co in **4** while a slightly higher distortion (CShM = 0.992 (**5**), 0.946 (**6**)) was observed compared to other trivalent Co in **5** and **6**. For a detailed discussion of various bonding parameters around the Co centers, refer to the ESI.† The crystal lattices for all the three clusters **4–6** exhibited voids which may be accessed by solvent molecules. These voids make up 19.6%, 21.8% and 22.6% of the volume of the unit cell in **4**, **5** and **6**, respectively. Fig. S7 and S8† show the crystal packing diagrams along

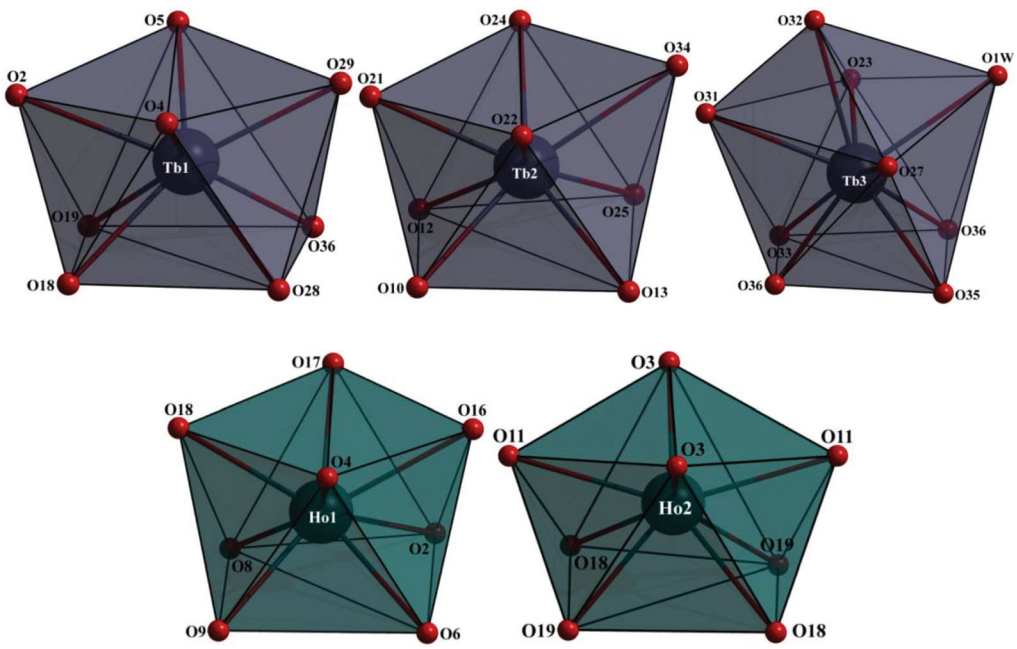

Fig. 7 Various geometries around Tb1, Tb2 (Distorted Square Antiprism (SAPR)) and Tb3 (Distorted Muffin (MFF)) in **4** (top) and Ho1 (Distorted Square Antiprism (SAPR)) and Ho2 (Distorted Triangular Dodecahedron (TDD)) in **6** (bottom).

Published on 22 June 2021. Downloaded by Goteborgs Universitet on 9/1/2021 4:56:06 AM.

the *c* axis and representations of such voids in **4** and **6** respectively.

Due to the absence of solvent molecules in the crystal lattice only intra molecular hydrogen bonding is observed in **4–6** (Table S5 and Fig. S9†) which lends stability to these large clusters. In **6**, two μ_3-OH^- bridges (O15 and O16) in each cube show hydrogen bonding interaction with O1 of the phenoxido group (O15···O1, 2.723(13) Å) and O14 of η^2-pivalate from the other cube. The third μ_3-OH^- bridge (O17) has interaction with the μ_3 as well as μ_2-OH^- bridges (O18 and O19) in the curved chain (O17···O18, 2.953(14) Å; O17···O19, 2.779(15) Å). The μ_3 and μ_2-OH^- bridges (O18 and O19) are further hydrogen bonded to the pivalate (coordinating Ho2) O11 and O12 (O18···O11, 3.07(2) Å; O19···O12, 3.02(3) Å).

Investigation of aggregation processes and structural transformation

In order to understand the aggregation pathway leading to the formation of the clusters **1** and **3**, high-resolution mass spectrometry (HRMS) (+ve) was performed in MeOH (reaction mixtures) to identify possible logical intermediates. Further analysis of HRMS (+ve) patterns of **1**, **2** and **3** in MeCN revealed the formation of new intermediate species responsible for an altered course of aggregation for the formation of high nuclearity clusters **4**, **5** and **6**. Such investigations highlighted the role of the bridging OMe^- in directing the pathway for aggregation and hence the ultimate structure of the clusters.

Analysis of the mass spectra of **1** and **3** in MeOH revealed a peak at *m*/*z* = **773.1844** (Fig. S10 and S11†) which can be assigned to the dinuclear mixed valent $Co^{II}Co^{III}$ species $\{[Co^{II}Co^{III}L1(O_2CCMe_3)_3(OMe)(H_2O)_2]\cdot 2CH_3OH\cdot H_2O + K + H\}^+$ ($C_{27}H_{54}Co_2KNO_{14}$; calcd 773.1840). The ligand anion $L1^{2-}$ initially coordinates to one of the cobalt centers of $Co_2(\mu\text{-}OH_2)(O_2CCMe_3)_4(HO_2CCMe_3)_4$ and at the same time bridges the second using its alkoxido arm giving rise to such dinuclear species (Scheme 2, species **a**). A OMe^- bridge (derived from the solvent) between the cobalt centers stabilizes the species. Peaks at *m*/*z* = **1013.2030** and **1019.2080** could be further observed for **1** and **3**, respectively, which are assignable to the trinuclear fragments $\{[Tb^{III}Co^{II}Co^{III}L1(O_2CCMe_3)_3(HO_2CCMe_3)_2(OMe)(OH)_2] + H\}^+$ ($C_{35}H_{62}Co_2NO_{15}Tb$; calcd, 1013.2032) and $\{[Ho^{III}Co^{II}Co^{III}L1(O_2CCMe_3)_3(HO_2CCMe_3)_2(OMe)(OH)_2] + H\}^+$ ($C_{35}H_{62}Co_2NO_{15}Ho$; calcd, 1019.2082). The initially formed dinuclear $Co^{II}Co^{III}$ species traps a Ln^{III} ion using the dangling $Me_3CCO_2^-$ groups and OH^- bridges (the two coordinated H_2O molecules are prone to hydrolysis) to form such trinuclear $\{Co_2Ln\}$ species (Scheme 2, species **b**). The ultimate heptanuclear dicubane $Ln^{III}_3Co^{II}_2Co^{III}_2$ core structure is generated by the trapping of a second Ln^{III} ion at the vertex shared position by two $\{Co_2Ln\}$ units *via* extension of the bridging capacity of OH^- and OMe^- from μ_2 to μ_3 (Scheme 2, intermediate **c**). The bridging OMe^- is important for not only stabilizing the initial dinuclear $Co^{II}Co^{III}$ species but also in trapping the vertex shared Ln^{III} hence having a major directing role in the aggregation process which will be further exemplified in the following dis-

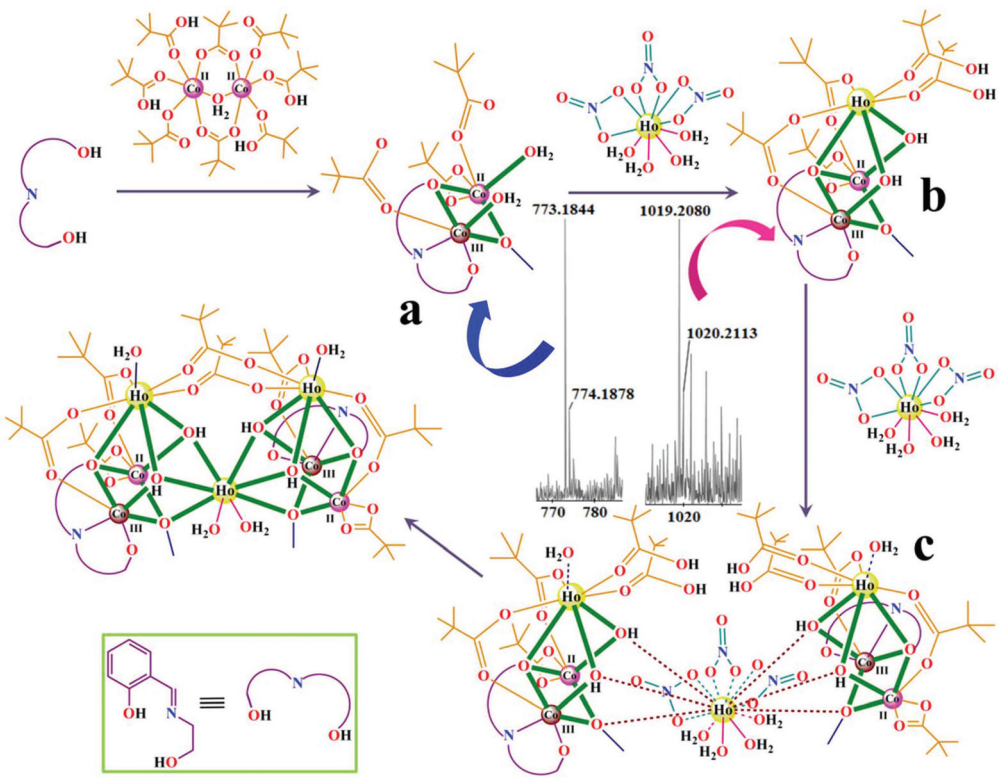

Scheme 2 Proposed pathway of aggregation for the formation of **3** in MeOH.

This journal is © The Royal Society of Chemistry 2021

Published on 22 June 2021. Downloaded by Goteborgs Universitet on 9/1/2021 4:56:06 AM.

cussions. The formation of anionic mononuclear lanthanide carboxylate species in solution could be detected in their protonated forms as $\{[Tb^{III}(O_2CCMe_3)_4(MeOH)_2]\cdot H_2O + 2H\}^+$ ($C_{22}H_{48}O_{11}Tb$; calcd 647.2445) and $\{[Ho^{III}(O_2CCMe_3)_4(MeOH)_2]\cdot H_2O + 2H\}^+$ ($C_{22}H_{48}O_{11}Ho$; calcd 653.2495) at m/z = **647.2440** and **653.2490** for **1** and **3**, respectively. Coordination of $Me_3CCO_2^-$, released from $Co_2(\mu\text{-}OH_2)(O_2CCMe_3)_4(HO_2CCMe_3)_4$ following ligand binding, to Ln^{III} ions leads to the formation of these unique and literature unknown anions essential for the crystallization and charge balance of monocationic $\{Ln^{III}_3Co^{II}_2Co^{III}_2\}^+$ clusters.

The HRMS spectra of **1**, **2** and **3** in MeCN (Fig. S12–S14†) exhibit peaks at m/z = **831.0720, 931.1343** and **937.1407** respectively assignable to trinuclear species $\{[Tb^{III}Co^{II}Co^{III}L1(O_2CCMe_3)_3(OH)_2(H_2O)_3]\}^+$ ($C_{24}H_{44}Co_2NO_{13}Tb$; calcd 831.0725), $\{[Dy^{III}Co^{II}Co^{III}L1(O_2CCMe_3)_3(OH)_2(H_2O)_3]\cdot CH_3CN\cdot 3H_2O\}^+$ ($C_{26}H_{53}Co_2N_2O_{16}Dy$; calcd 931.1346) and $\{[Ho^{III}Co^{II}Co^{III}L1(O_2CCMe_3)_3(OH)_2(H_2O)_3]\cdot 2CH_3CN\cdot H_2O\}^+$ ($C_{28}H_{52}Co_2N_3O_{14}Ho$; calcd 937.1411) (Scheme 3, species **a**). Such trinuclear species **a** arise following the collapse of the heptanuclear dicubane cationic cluster in **1–3** due to the loss of the vertex-shared Ln^{III} ion along with the bridging OMe^-. In our previous investigation we

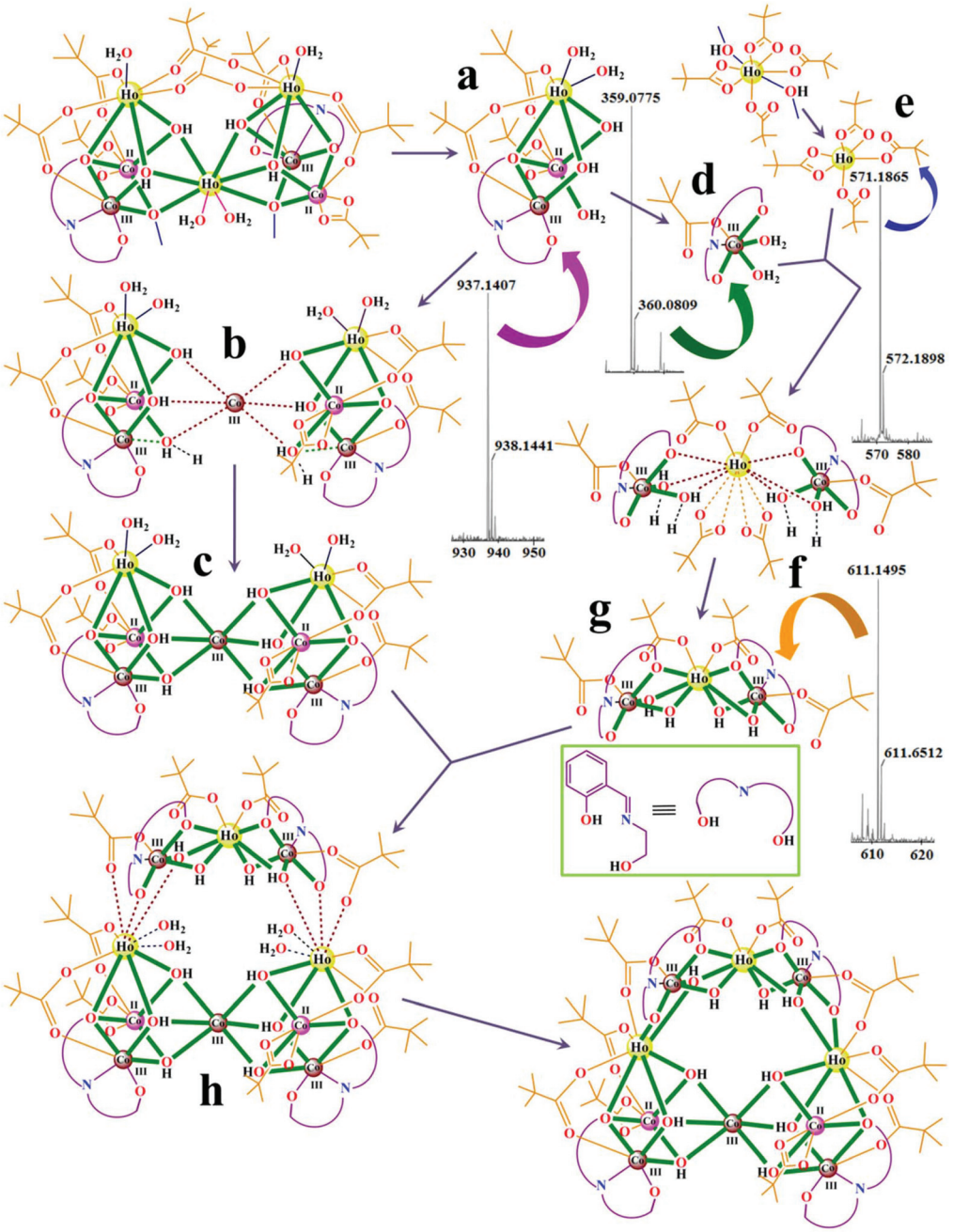

Scheme 3 Proposed aggregation pathway for the transformation of **3** into **6** in MeCN.

Published on 22 June 2021. Downloaded by Goteborgs Universitet on 9/1/2021 4:56:06 AM.

had shown that the higher dielectric constant of MeCN favors the substitution of bridging OMe^- with a water molecule,[4a] the likes of which is observed here as well. In its absence the trapping of a Ln^{III} ion at the shared vertex position is not favorable; instead, the OH^- bridge generated through hydrolysis of the water molecule shows preference towards a 3d metal ion. Two species **a** moieties thus trap a $Co^{II/III}$ ion at the vertex shared position *via* increase of the bridging capacity of the OH^- ions (Scheme 3, intermediate **b**) probably leading to the formation of vertex-shared dicubane cluster like species **c** shown in Scheme 3. In the absence of a –OMe function on the ligand, the species **a** cannot rearrange as observed in our previous work.

Further scrutiny of the HRMS patterns in MeCN revealed a peak at m/z = **359.0775** in **1–3** which can be assigned to the mononuclear species $\{Co^{III}L1(O_2CCMe_3)(H_2O)\}^{\bullet+}$ ($C_{14}H_{22}CoNO_6$; calcd 359.0774) (Scheme 3, species **d**). The loss of the OMe^- bridge also destabilizes the trinuclear species **a**, a portion of which further collapses forming the mononuclear species **d**. The spectra also indicate the presence of the lanthanide–pivalate-based anion after loss of two MeOH in the form of protonated species $\{[Tb^{III}(O_2CCMe_3)_4] + 2H\}^+$ ($C_{20}H_{38}O_8Tb$; calcd 565.1815), $\{[Dy^{III}(O_2CCMe_3)_4] + 2H\}^+$ ($C_{20}H_{38}O_8Dy$; calcd 570.1853) and $\{[Ho^{III}(O_2CCMe_3)_4] + 2H\}^+$ ($C_{20}H_{38}O_8Ho$; calcd 571.1865) (Scheme 3, species **e**) at m/z = **565.1819**, **570.1848** and **571.1865**. Also present in the spectra are peaks at m/z = **608.1114**, **693.1525** and **611.1495** corresponding to heteronuclear species $\{[Tb^{III}Co^{III}_2L1_2(O_2CCMe_3)_3(OH)_4(H_2O)]\cdot 4CH_3CN\cdot H_2O + K + 3H\}^{2+}$ ($C_{41}H_{68}Co_2KN_6O_{16}Tb$; calcd 608.1118), $\{[Dy^{III}Co^{III}_2L1_2(O_2CCMe_3)_4(OH)_4]\cdot 5CH_3CN\cdot 2H_2O + K + Na + 3H\}^{2+}$ ($C_{48}H_{80}Co_2KN_7NaO_{18}Dy$; calcd 693.1520) and $\{[Ho^{III}Co^{III}_2L1_2(O_2CCMe_3)_4(OH)_4]\cdot 2CH_3CN\cdot 3H_2O + 5H\}^{2+}$ ($C_{42}H_{75}Co_2N_4O_{19}Ho$; calcd 611.1491) (Scheme 3, species **g**). Two mononuclear species **d** trap the lanthanide–pivalate anion (species **e**) *via* μ_2 bridging phenoxido and OH^- groups (generated through hydrolysis of coordinated water) (Scheme 3, intermediate **f**) to form the trinuclear heterometallic species **g**. This trinuclear chain further attaches itself to the proposed dicubane species **c** at the two Ln^{III} vertices (Scheme 3, species **h**) by utilizing a μ_2 bridging coordination of the alkoxido groups at both ends, while at the same time extending a μ_3 bridging mode of two OH^- groups along with capping $\mu_{1,3}$ coordination of two terminal $Me_3CCO_2^-$ to give rise to the final decanuclear cluster $Ln^{III}_3Co^{II}_{3/2}Co^{III}_{4/5}$.

Magnetic properties

Magnetic susceptibility measurements were carried out on the samples from 290 to 2 K (Fig. 8). At ambient temperature, $\chi_M T$ = 53.4 $cm^3\ mol^{-1}$ K for **1** and 61.6 $cm^3\ mol^{-1}$ K for **3**, consistent with the calculated values for uncoupled spins (53.1 $cm^3\ mol^{-1}$ K and 62.1 $cm^3\ mol^{-1}$ K, respectively) for two Co(II) centers and four Ln(III) centers (Co(II) g = 2.5, S = 3/2 and Tb(III) g = 3/2, J = 6 for **1** and Co(II) g = 2.5, S = 3/2 and Ho(III) g = 1.25, J = 8 for **3**). Upon cooling the $\chi_M T$ value shows a marginal decrease up to 90 K and then decreases more prominently to have values of 25.9 $cm^3\ mol^{-1}$ K and 29.5 $cm^3\ mol^{-1}$ K for **1** and **3**, respectively, at 2 K. This behavior is consistent with the thermal depopulation of the split energy levels of anisotropic Co_2^+ and Ln^{3+} ions at lower temperatures. Spin–orbit coupling splits the $^4T_{1g}$ term in Co^{II} while for the Ln^{III} ions contribution to the magnetic properties arises from $2J + 1$ energy states. In addition very weak mostly antiferromagnetic interactions between the metal ion centers may affect the curve at the lowest temperatures as observed for the Dy analogue **2**.[4a] The magnetization of the complexes was studied under a dc field from 0 to 7 T. Both analogues do not reach saturation, with $M/N\beta$ = 24.3 for **1** and $M/N\beta$ = 26.6 for **3**, at 2 K and 7 Tesla, consistent with strong magnetic anisotropy. Neither complex shows slow magnetic relaxation in ac susceptibility studies.

For **4–6**, we were unable to synthesize magnetically pure bulk products from which publishable magnetic data could be extracted. Preliminary investigations showed no slow magnetic relaxation in ac susceptibility studies.

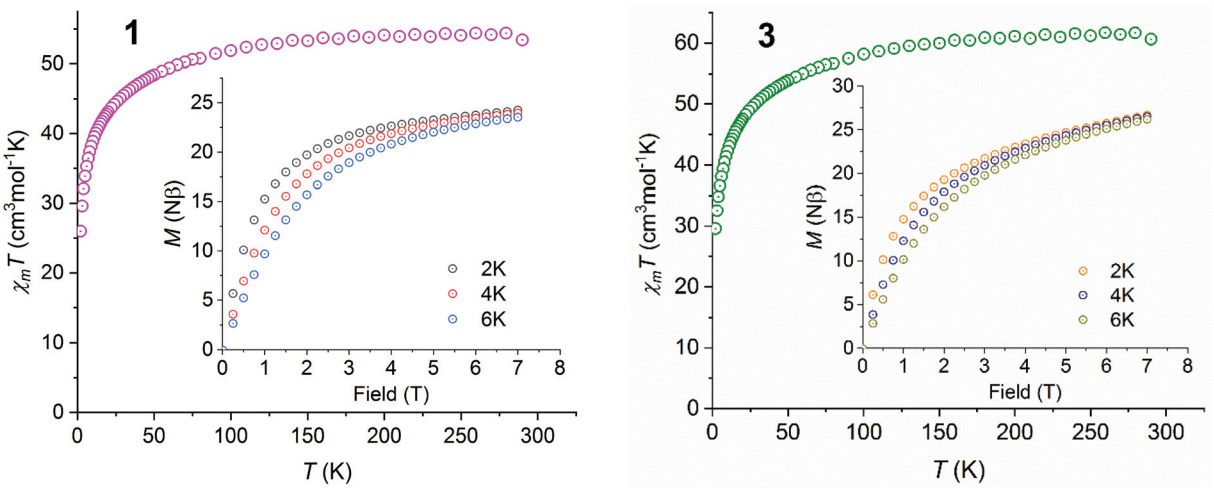

Fig. 8 Temperature dependence of $\chi_M T$ and magnetization *vs.* field data at 2, 4 and 6 K (inset) for **1** and **3**.

 This journal is © The Royal Society of Chemistry 2021

Published on 22 June 2021. Downloaded by Goteborgs Universitet on 9/1/2021 4:56:06 AM.

Conclusions

The presented syntheses of Co_4Ln_3 and Co_7Ln_3 type coordination aggregates highlighted the role of the parent ligand anion, *in situ* generated and metal ion salt derived co-ligands and solvent in the synthesis route, which exploits the varying possibilities of condensation reactions. The coordination-induced aggregation processes were explored for $Co_2(\mu\text{-}OH_2)(O_2CCMe_3)_4(HO_2CCMe_3)_4$ and lanthanide nitrate salts in the presence of $L1^{2-}$. Base-assisted *in situ* generation of OMe^- and OH^- bridges from direct supports of $L1^{2-}$ provided heptanuclear 3d–4f aggregates having cationic $\{Ln^{III}_3Co^{II}_2Co^{III}_2\}$ cores in **1** and **3** giving vertex-shared dicubane structures, where the vertex-shared position was occupied by a Ln^{III} ion. *In situ* generation of unique lanthanide–pivalate-based anions, $Ln(\eta^1\text{-}O_2CCMe_3)_2(\eta^2\text{-}O_2CCMe_3)_2(CH_3OH)_2^-$, was essential for the crystallization of the cationic heptanuclear clusters. Solvent-assisted structural disintegration and re-aggregation following a different pathway took place when these heptanuclear clusters were treated with MeCN to provide decanuclear **4–6** having neutral $\{Ln^{III}_3Co^{II}_{3/2}Co^{III}_{4/5}\}$ cores. Dissolution of **1–3** in MeCN lead to the removal of the OMe^- bridges and central Ln^{III} ion, which were replaced by OH^- bridges and $Co^{II/III}$ ions, respectively, in the dicubane part of the high nuclearity clusters **4–6**. Additionally the lanthanide–pivalate-based anion is trapped by mononuclear $\{Co^{III}L1\}$ type species to form the curved chain connecting the two cubic halves. Analysis of HRMS (+ve) patterns of the heptanuclear clusters in MeOH and MeCN revealed the aggregation pathways and an altered route of aggregation for the formation of the high nuclearity clusters **4–6**.

Conflicts of interest

The authors declare no competing financial interests.

Acknowledgements

DB is thankful towards IIT Kharagpur for the research facilities and his fellowship.

References

1 (*a*) A. Shyamal and D. Kumar, *J. Less-Common Met.*, 1980, **71**, 113–117; (*b*) O. Stetsiuk, N. Plyuta, N. Avarvari, E. Goreshnik, V. Kokozay, S. Petrusenko and A. Ozarowski, *Cryst. Growth Des.*, 2020, **20**, 1491–1502; (*c*) L. E. H. Paul, I. C. Foehn, A. Schwarzer, E. Brendler and U. Böhme, *Inorg. Chim. Acta*, 2014, **423**, 268–280; (*d*) S. Majumder, J. P. Naskar, A. Bhattacharya, R. Ganguly, P. Saha and S. Chowdhury, *J. Coord. Chem.*, 2015, **68**, 599–615; (*e*) H. Hoepfl, M. Sanchez, V. Barba, N. Farfan, S. Rojas and R. Santillan, *Inorg. Chem.*, 1998, **37**, 1679–1692; (*f*) A. Sieber, C. Boskovic, R. Bircher, O. Waldmann, S. T. Ochsenbein, G. Chaboussant, H. U. Guedel, N. Kirchner, J. v. Slageren and W. Wernsdorfer, *Inorg. Chem.*, 2005, **44**, 4315–4325; (*g*) C. Boskovic, A. Sieber, G. Chaboussant, H. U. Guedel, J. Ensling, W. Wernsdorfer, A. Neels, G. Labat, H. Stoeckli-Evans and S. Janssen, *Inorg. Chem.*, 2004, **43**, 5053–5068.

2 (*a*) M. Das, S. R. Chaudhuri, D. Basak, S. Dasgupta and D. Ray, *Inorg. Chim. Acta*, 2019, **485**, 140–154; (*b*) M. Das, D. Basak, Z. Travnicek, J. Vanco and D. Ray, *Chem. – Asian J.*, 2019, **14**, 3898–3914; (*c*) M. Das, G. A. Craig, D. Escudero, M. Murrie, A. Frontera and D. Ray, *New J. Chem.*, 2018, **42**, 14349–14364; (*d*) M. Das, R. Herchel, Z. Travnicek, V. Bertolasi and D. Ray, *New J. Chem.*, 2018, **42**, 16717–16728; (*e*) K. Chattopadhyay, G. A. Craig, M. J. H. Ojea, M. Pait, A. Kundu, J. Lee, M. Murrie, A. Frontera and D. Ray, *Inorg. Chem.*, 2017, **56**, 2639–2652; (*f*) K. Chattopadhyay, G. A. Craig, A. Kundu, V. Bertolasi, M. Murrie and D. Ray, *Inorg. Chem.*, 2016, **55**, 10783–10792; (*g*) M. Pait, M. Shatruk and D. Ray, *Dalton Trans.*, 2015, **44**, 11741–11754; (*h*) A. K. Ghosh, T. S. Mahapatra, R. Clerac, C. Mathoniere, V. Bertolasi and D. Ray, *Inorg. Chem.*, 2015, **54**, 5136–5138; (*i*) M. Pait, A. Bauza, A. Frontera, E. Colacio and D. Ray, *Inorg. Chem.*, 2015, **54**, 4709–4723; (*j*) M. Pait, E. Colacio and D. Ray, *Polyhedron*, 2015, **88**, 90–100; (*k*) S. Nayak, G. Aromi, S. J. Teat, J. R.-Arino, P. Gamez and J. Reedijk, *Dalton Trans.*, 2010, **39**, 4986–4990; (*l*) E. Pilichos, A. Escuer, M. F. Bardia and J. Mayans, *Chem. – Eur. J.*, 2020, **26**, 13053–13062; (*m*) A. K. Ghosh, M. Shatruk, V. Bertolasi, K. Pramanik and D. Ray, *Inorg. Chem.*, 2013, **52**, 13894–13903; (*n*) M. Mitra, P. Raghavaiah and R. Ghosh, *New J. Chem.*, 2015, **39**, 200–205; (*o*) D. Saha, T. Maity, R. Bera and S. Koner, *Polyhedron*, 2013, **56**, 230–236.

3 D. Basak, J. v. Leusen, T. Gupta, P. Kögerler, V. Bertolasi and D. Ray, *Inorg. Chem.*, 2020, **59**(4), 2387–2405 and references therein.

4 (*a*) D. Basak, J. v. Leusen, T. Gupta, P. Kögerler and D. Ray, *Dalton Trans.*, 2020, **49**, 7576–7591; (*b*) H. Wei, C.-L. Wang, W. Gao, J.-P. Liu and X.-M. Zhang, *CrystEngComm*, 2020, **22**, 7639–7647; (*c*) M. N. Akhtar, M. A. AlDamen, J. Khan, M. Shahid and A. M. Kirillov, *Cryst. Growth Des.*, 2020, **20**, 6545–6554; (*d*) Y. Wang, Z. Yuan, H. Ren, W. Xu, J. Xu, H. Zhang, J. Sha and H. Zhang, *Inorg. Chim. Acta*, 2020, **511**, 119786.

5 (*a*) R. E. P. Winpenny, *J. Chem. Soc., Dalton Trans.*, 2002, 1–10; (*b*) Z. Zheng, *Chem. Commun.*, 2001, 2521–2529; (*c*) R. Robson, *Dalton Trans.*, 2008, 5113–5131; (*d*) C. Papatriantafyllopoulou, E. E. Moushi, G. Christou and A. J. Tasiopoulos, *Chem. Soc. Rev.*, 2016, **45**, 1597–1628; (*e*) X. Yang, C. Chan, D. Lam, D. Schipper, J. M. Stanley, X. Chen, R. A. Jones, B. J. Holliday, W.-K. Wong, S. Chen and Q. Chen, *Dalton Trans.*, 2012, **41**, 11449–11453; (*f*) T. C. Stamatatos, C. G. Efthymiou, C. C. Stoumpos and S. P. Perlepes, *Eur. J. Inorg. Chem.*, 2009, 3361–3391; (*g*) J. M. Frost, F. J. Kettles, C. Wilson and M. Murrie, *Dalton Trans.*, 2016, **45**, 18094–18097.

Published on 22 June 2021. Downloaded by Goteborgs Universitet on 9/1/2021 4:56:06 AM.

6 (*a*) H.-L. Zheng, X.-L. Chen, T. Li, Z. Yin, Y. Zhang, M. Kurmoo and M.-H. Zeng, *Chem. – Eur. J.*, 2018, **24**, 7906–7912; (*b*) H. X. Na, P. Y. Yang, Z. Yin, Y. H. Wang, L. X. Chang, R. Si, M. Kurmoo and M. H. Zeng, *Chem. – Eur. J.*, 2016, **22**, 18404–18411; (*c*) Y.-Q. Hu, M.-H. Zeng, K. Zhang, S. Hu, F.-F. Zhou and M. Kurmoo, *J. Am. Chem. Soc.*, 2013, **135**, 7901–7908.

7 (*a*) H. N. Miras, E. F. Wilson and L. Cronin, *Chem. Commun.*, 2009, 1297–1311; (*b*) X. L. Chen, H. B. Xu, X. X. Shi, Y. Zhang, T. Yang, M. Kurmoo and M. H. Zeng, *Inorg. Chem.*, 2017, **56**, 14069–14076; (*c*) T. Zhang, L.-P. Zhou, X.-Q. Guo, L.-X. Cai and Q.-F. Sun, *Nat. Commun.*, 2017, **8**, 15898; (*d*) G. J. T. Cooper, G. N. Newton, P. Kögerler, D.-L. Long, L. Engelhardt, M. Luban and L. Cronin, *Angew. Chem., Int. Ed.*, 2007, **46**, 1340–1344; (*e*) G. N. Newton, G. J. T. Cooper, P. Kögerler, D.-L. Long and L. Cronin, *J. Am. Chem. Soc.*, 2008, **130**, 790–791.

8 (*a*) M. Du, X.-H. Bu, Y.-M. Guo and J. Ribas, *Chem. – Eur. J.*, 2004, **10**, 1345–1354; (*b*) A. K. Gupta and A. Orthaber, *Cryst. Growth Des.*, 2020, **20**, 4232–4237; (*c*) X.-M. Luo, N.-F. Li, Q.-F. Lin, J.-P. Cao, P. Yuan and Y. Xu, *Inorg. Chem. Front.*, 2020, **7**, 2072–2079; (*d*) X.-F. Ma, H.-L. Wang, Z.-H. Zhu, B. Li, K.-Q. Mo, H.-H. Zou and F.-P. Liang, *Dalton Trans.*, 2019, **48**, 11338–11344; (*e*) M. Chen, M. Zhang, X. Wang, Y. Bi, B. Chen and Z. Zheng, *Inorg. Chem.*, 2019, **58**, 6276–6282; (*f*) Z. Chen, Y. Shen, L. Li, H. Zou, X. Fu, Z. Liu, K. Wang and F. Liang, *Dalton Trans.*, 2017, **46**, 15032–15039; (*g*) Y. Zhou, X.-Y. Zheng, J. Cai, Z.-F. Hong, Z.-H. Yan, X.-J. Kong, Y.-P. Ren, L.-S. Long and L.-S. Zheng, *Inorg. Chem.*, 2017, **56**, 2037–2041.

9 K. C. Mondal, A. Sundt, Y. Lan, G. E. Kostakis, O. Waldmann, L. Ungur, L. F. Chibotaru, C. E. Anson and A. K. Powell, *Angew. Chem., Int. Ed.*, 2012, **51**, 7550–7554.

10 (*a*) P.-P. Yang, X.-L. Wang, L.-C. Li and D.-Z. Liao, *Dalton Trans.*, 2011, **40**, 4155–4161; (*b*) R. Modak, Y. Sikdar, G. Cosquer, S. Chatterjee, M. Yamashita and S. Goswami, *Inorg. Chem.*, 2016, **55**, 691–699.

11 (*a*) H.-J. Lun, M.-H. Du, D.-H. Wang, X.-J. Kong, L.-S. Long and L.-S. Zheng, *Inorg. Chem.*, 2020, **59**, 7900–7904; (*b*) Q. Lin, J. Li, Y. Dong, G. Zhou, Y. Song and Y. Xu, *Dalton Trans.*, 2017, **46**, 9745–9749; (*c*) X.-Y. Zheng, S.-Q. Wang, W. Tang, G.-L. Zhuang, X.-J. Kong, Y.-P. Ren, L.-S. Long and L.-S. Zheng, *Chem. Commun.*, 2015, **51**, 10687–10690; (*d*) J.-B. Peng, Q.-C. Zhang, X.-J. Kong, Y.-Z. Zheng, Y.-P. Ren, L.-S. Long, R.-B. Huang, L.-S. Zheng and Z. Zheng, *J. Am. Chem. Soc.*, 2012, **134**, 3314–3317.

12 (*a*) K. S. Pedersen, J. Dreiser, H. Weihe, R. Sibille, H. V. Johannesen, M. A. Sørensen, B. E. Nielsen, M. Sigrist, H. Mutka, S. Rols, J. Bendix and S. Piligkos, *Inorg. Chem.*, 2015, **54**, 7600–7606; (*b*) F. Ortu, D. Reta, Y.-S. Ding, C. A. P. Goodwin, M. P. Gregson, E. J. L. McInnes, R. E. P. Winpenny, Y.-Z. Zheng, S. T. Liddle, D. P. Mills and N. F. Chilton, *Dalton Trans.*, 2019, **48**, 8541–8545; (*c*) W. Huang, F.-X. Shen, S.-Q. Wu, L. Liu, D. Wu, Z. Zheng, J. Xu, M. Zhang, X.-C. Huang, J. Jiang, F. Pan, Y. Li, K. Zhu and O. Sato, *Inorg. Chem.*, 2016, **55**, 5476–5484; (*d*) W. Wernsdorfer, N. A. Alcalde, D. N. Hendrickson and G. Christou, *Nature*, 2002, **416**, 406–409.

13 (*a*) S. Paul, R. Clérac, N. G. R. Hearns and D. Ray, *Cryst. Growth Des.*, 2009, **9**, 4032–4040; (*b*) R. Lee, A. I. Kamiyama, H. Motoyoshi and T. Konno, *CrystEngComm*, 2012, **14**, 1936–1938; (*c*) D. Liu, H.-X. Li, Z.-G. Ren, Y. Chen, Y. Zhang and J.-P. Lang, *Cryst. Growth Des.*, 2009, **9**, 4562–4566; (*d*) H.-P. Xiao, J. Zhou, X.-L. Wang, H.-H. Zou, R.-Q. Zhao and H. Xiao, *Dalton Trans.*, 2014, **43**, 12306–12312.

14 J.-S. Lu and R. Wang, in *The rare earth elements: Fundamentals and applications*, ed. D. A. Atwood, Wiley, 2012, Carboxylate, pp. 229.

15 (*a*) H. Ke, L. Zhao, Y. Guo and J. Tang, *Dalton Trans.*, 2012, **41**, 9760–9765; (*b*) L. Zhao, J. Wu, S. Xue and J. Tang, *Chem. – Asian J.*, 2012, **7**, 2419–2423; (*c*) M. C. Majee, S. M. T. Abtab, D. Mondal, M. Maity, M. Weselski, M. Witwicki, A. Bieńko, M. Antkowiak, G. Kamieniarz and M. Chaudhury, *Dalton Trans.*, 2018, **47**, 3425–3439.

16 L. F. Zou, L. Zhao, Y. N. Guo, G. M. Yu, Y. Guo, J. K. Tang and Y. H. Li, *Chem. Commun.*, 2011, **47**, 8659–8661.

17 G. Aromi, A. S. Batsanov, P. Christian, M. Helliwell, A. Parkin, S. Parsons, A. A. Smith, G. A. Timco and R. E. P. Winpenny, *Chem. – Eur. J.*, 2003, **9**, 5142–5161.

18 Saint, *Smart and XPREP*, Siemens Analytical X-ray Instruments Inc., Madison, WI, 1995.

19 G. M. Sheldrick, *SHELXS-2014*, University of Göttingen, Göttingen, Germany, 2014.

20 G. M. Sheldrick, *Acta Crystallogr., Sect. C: Struct. Chem.*, 2015, **71**, 3–8.

21 L. J. Farrugia, *J. Appl. Crystallogr.*, 2012, **45**, 849–854.

22 O. V. Dolomanov, L. J. Bourhis, R. J. Gildea, J. A. K. Howard and H. Puschmann, *J. Appl. Crystallogr.*, 2009, **42**, 339–341.

23 G. M. Sheldrick, *SADABS Software for Empirical Absorption Correction*, University of Göttingen, Institute fur Anorganische Chemieder Universitat, Göttingen, Germany, 1999–2003.

24 *DIAMOND, Visual Crystal Structure Information System, version 3.1*, Crystal Impact, Bonn, Germany, 2004.

25 I. D. Brown and D. Altermatt, *Acta Crystallogr., Sect. B: Struct. Sci.*, 1985, **41**, 244–247.

26 I. D. Brown, *Chem. Rev.*, 2009, **109**, 6858–6919.

This journal is © The Royal Society of Chemistry 2021